Matrix stiffness exacerbates the proinflammatory responses of vascular smooth muscle cell through the DDR1-DNMT1 mechanotransduction axis

Jin Wang [a,b,c,1], Si-an Xie [a,b,c,d,1], Ning Li [e,f], Tao Zhang [g], Weijuan Yao [a], Hucheng Zhao [h], Wei Pang [a], Lili Han [a], Jiayu Liu [a,b,c], Jing Zhou [a,b,c,*]

[a] Department of Physiology and Pathophysiology, School of Basic Medical Sciences, Hemorheology Center, School of Basic Medical Sciences, Peking University, Beijing, PR China
[b] Key Laboratory of Molecular Cardiovascular Science, Ministry of Education, Beijing, PR China
[c] National Health Commission Key Laboratory of Cardiovascular Molecular Biology and Regulatory Peptides; Beijing Key Laboratory of Cardiovascular Receptors Research, Peking University, Beijing, PR China
[d] Department of Gastroenterology, Beijing Friendship Hospital, Capital Medical University, National Clinical Research Center for Digestive Disease, Beijing Digestive Disease Center, Beijing Key Laboratory for Precancerous Lesion of Digestive Disease, Beijing, PR China
[e] Center for Biomechanics and Bioengineering, Key Laboratory of Microgravity (National Microgravity Laboratory), And Beijing Key Laboratory of Engineered Construction and Mechanobiology, Institute of Mechanics, Chinese Academy of Sciences, Beijing, PR China
[f] School of Engineering Sciences, University of Chinese Academy of Sciences, Beijing, PR China
[g] Department of Vascular Surgery, Peking University People's Hospital, Beijing, PR China
[h] Institute of Biomechanics and Medical Engineering, School of Aerospace Engineering, Tsinghua University, Beijing, PR China

ARTICLE INFO

ABSTRACT

Vascular smooth muscle cell (vSMC) is highly plastic as its phenotype can change in response to mechanical cues inherent to the extracellular matrix (ECM). VSMC may be activated from its quiescent contractile phenotype to a proinflammatory phenotype, whereby the cell secretes chemotactic and inflammatory cytokines, e.g. MCP1 and IL6, to functionally regulate monocyte and macrophage infiltration during the development of various vascular diseases including arteriosclerosis. Here, by culturing vSMCs on polyacrylamide (PA) substrates with variable elastic moduli, we discovered a role of discoidin domain receptor 1 (DDR1), a receptor tyrosine kinase that binds collagens, in mediating the mechanical regulation of vSMC gene expression, phenotype, and proinflammatory responses. We found that ECM stiffness induced DDR1 phosphorylation, oligomerization, and endocytosis to repress the expression of DNA methyltransferase 1 (DNMT1), very likely in a collagen-independent manner. The DDR1-to-DNMT1 signaling was sequentially mediated by the extracellular signal-regulated kinases (ERKs) and p53 pathways. ECM stiffness primed vSMC to a proinflammatory phenotype and this regulation was diminished by DDR1 inhibition. In agreement with the in vitro findings, increased DDR1 phosphorylation was observed in human arterial stiffening. DDR1 inhibition in mouse attenuated the acute injury or adenine diet-induced vascular stiffening and inflammation. Furthermore, mouse vasculature with SMC-specific deletion of Dnmt1 exhibited proinflammatory and stiffening phenotypes. Our study demonstrates a role of SMC DDR1 in perceiving the mechanical microenvironments and down-regulating expression of DNMT1 to result in vascular pathologies and has potential implications for optimization of engineering artificial vascular grafts and vascular networks.

1. Introduction

Vascular smooth muscle cell (vSMC) is highly plastic as its phenotype can change in response to the integration of multiple environmental stimuli [1]. Increasing evidence suggests that mechanical cues inherent to the wall extracellular matrix (ECM) may act solely or synergistically with some biochemical factors to modulate the phenotype of vSMCs [2–4], hinting at an impact of vessel mechanical properties on vascular

function. In physiological conditions, the stiffness (elastic modulus) of mammalian blood vessels is usually 2–5 kPa, whereas in a variety of common chronic vascular inflammatory diseases, including atherosclerosis, arteriosclerosis, hypertension, and post-operative stenosis, the elastic modulus of arterial walls can dramatically increase, reaching up to 96 kPa [5]. VSMCs residing in the diseased vessels take on a "synthetic" and "proinflammatory" phenotype, whereby cell contractility is compromised, and cell proliferation, migration and inflammation are induced [6]. The proinflammatory SMCs can secrete chemotactic factors and cytokines, e.g. MCP1, IL6 and IL8, to functionally regulate monocyte and macrophage infiltration during the development of vascular pathologies [6,7]. Indeed, a remarkable correlation has been found between wall stiffness and vascular inflammation [8–10], whereas the potential causal relationship and underlying mechanisms remain undecided.

DNA methylation is an epigenetic mechanism involving the covalent methylation of the C5 position of cytosine residues (5-C) to form 5-methylcytosine (5-mC), in most cases resulting in the transcriptional repression of genes and noncoding genomic regions and less frequently coupling with transcriptional activation [11]. Maintenance of methylation patterns during cell replication is mediated by DNA methyltransferase 1 (DNMT1), which catalyzes the transfer of a methyl group from S-adenosyl methionine to hemi-methylated DNA [11]. We [2] and others [12,13] have reported DNA hypomethylation and insufficient DNMT1 expression in arteriosclerosis and atherosclerotic lesions, where dysregulation of SMC function and chronic wall inflammation occur. Pharmacological inhibition of DNMT1 has been indicated to induce the expression of cyclooxygenase-2 (COX-2) [14,15], whose deficiency decreased vascular stiffness and inflammation [16], suggestive of an anti-inflammatory activity of DNMT1. Several studies have documented the involvement of DNMT1 downregulation in phenotypic switch of vSMC in various aspects of these diseases [17]. Nevertheless, little is known about the pathways regulating DNMT1 expression that are initiated by the pathological environmental stimuli during disease development.

Our previous study has demonstrated that wall stiffness regulates vSMC phenotype via DNMT1 [2]. By culturing vSMCs on polyacrylamide (PA) substrates with variable elastic moduli, we found that substrate stiffness downregulated DNMT1 expression to cause DNA hypomethylation and vSMC osteogenic transdifferentiation regardless of the discrepancy of the coated-matrix proteins [2]. While our study identified DNMT1 as a mechanosensitive protein in vSMCs, our understanding of the mechanotransduction pathways remains rudimentary. Mechanotransduction usually involves several sequential steps: first, perceiving the mechanical forces by specific mechanosensors residing in the cell membrane or cytoskeleton; second, conversion of the mechanical forces to chemical activity; third, intracellular transmission of chemical signals or stresses if the forces are sensed by nuclear receptors instead of membrane receptors; and fourth, downstream biochemical signaling with cellular responses. Although there are some putative mechanosensors, e.g. integrins, ion channels, receptor tyrosine kinases (RTKs), G protein-coupled receptors, and focal adhesion, proposed to function in perceiving ECM stiffness in vSMCs [18,19], it remains unclear which mechanosensor is involved in transducing ECM mechanical cues to intracellular signaling pathways linked to regulation on DNMT1 expression.

The discoidin domain receptors (DDRs) are RTKs that undergo tyrosine autophosphorylation upon activation by various types of collagens [20]. The DDR family consists of two members, DDR1 and DDR2, both of which have been implicated in numerous physiological and pathological functions such as cell growth, differentiation and metabolism [21,22]. DDR1 was found to be expressed in epithelial cells, fibroblasts, oligodendrocytes, macrophages, and vSMCs [23]. Studies in fibroblasts, embryonic stem cells [24], and adipose stromal cells [25] have revealed a collagen-dependent DDR1 activation, i.e., phosphorylation (at Tyr792) and clustering, that mediates mechanotransduction

induced by ECM stiffness. Recent work also has identified a role of DDR1 as a mechanosensor in cultured vSMCs to perceive substrate stiffness [26]. However, to the best of our knowledge, no study has been conducted on elucidating whether collagen binding is required for the mechanical activation of DDR1.

Here, we elucidated how ECM stiffness orchestrates arterial inflammation and demonstrated a sequential pro-arteriogenic mechanism involving: (a) perception of matrix stiffness by DDR1, (b) the DDR1-to-DNMT1 signaling leading to downregulation of DNMT1 expression, and (c) chronic inflammation resulted from insufficient DNMT1 expression. Our study identifies a previously uncharacterized role of ECM stiffness in activating vSMC DDR1 to regulate the epigenome, and consequently, cell plasticity and vascular pathologies.

2. Materials and methods

2.1. Cell culture

Primary human umbilical artery SMCs, primary mouse aortic SMCs, RAW 264.7 macrophages, and HeLa cells were used in this study. Umbilical artery SMCs were cultured in F12 Nutrient Mixture F-12 Ham (Sigma) supplemented with 20% FBS (Gemini), 10% SMC Growth Medium (Cell Applications), and streptomycin. Mouse aortic SMCs, HeLa cells and RAW 264.7 cells were maintained in DMEM (GIBCO) supplemented with 10% FBS and streptomycin. Cells were maintained in a humidified incubator with 5% CO_2 at 37 °C. Primary SMCs at passage 3 to 7 were used in most of the experiments. To inhibit DDR1 activation, cells were incubated for 3 h with 10 μmol/L DDR1 inhibitor, DDR1-IN-1. To inhibit p53, cells were incubated for 24 h with 10 μmol/L PFT-α. To knockdown DNMT1 in SMCs, cells were infected with recombinant adenovirus expressing shRNA specifically targeting human DNMT1 genes (ad-shDNMT1). To inhibit the expression and activity of DNMT1, cells were incubated with 5-aza-2′-deoxycytidine (5-Aza) in culture medium at a concentration of 10 μmoL/L for three days with daily replacement of the medium. To inhibit the extracellular signal-regulated kinases (ERKs) activation, cells were treated for 24 h with 50 nmol/L PD98059.

2.2. Antibodies, inhibitors and recombinant protein

Rabbit polyclonal antibodies against DNMT1, p53, and DDR1, and mouse monoclonal antibody against Rab5A were purchased from Proteintech. Rabbit polyclonal antibodies against phosphorylated (phospho-) DDR1 (Tyr792) and phospho-p53 (Ser15), and rabbit monoclonal antibody against phospho-ERK1/2 were from CST. Mouse monoclonal antibodies against smooth muscle α-actin (SMA), ERK 1/2, and CD68 were from Santa Cruz Biotech, CallM, and Abcam, respectively. Rabbit polyclonal antibodies against MCP1 and GAPDH were from Abclonal and Easybio, respectively. DDR1 inhibitor DDR1-IN-1 was from Targetmol. p53 inhibitor PFT-α was from Cayman. Mitogen-activated protein kinase (MAPK) kinase/ERK pathway inhibitor PD98059 was from CST. DNMT inhibitor 5-Aza was from Selleck. The recombinant human DDR1: Fc protein was from R&D Systems.

2.3. Plasmids, transient transfection, and luciferase reporter assay

For knockdown of endogenous DDR1, cells at 80% confluence were transfected with siRNAs specific for DDR1 (# 1:5′- GAAUGUCGCUUCCGGCGUGUU-3′; # 2:5′- GAGCGUCUGUCUGCGGGUAUU-3′) or scrambled siRNA using lipofectamine 2000 transfection agent (Invitrogen) according to the manufacturer's instructions. For DNMT1 overexpression, cells were transfected with pcDNA3/Myc-DNMT1 that express full length of DNMT1, gifts from Arthur Riggs (Addgene plasmid # 36939) [27], or control plasmid pcDNA3, using lipofectamine 2000 transfection agent. P53 luciferase reporter plasmid was from YEASEN. PGL3 Luciferase reporter plasmid driven by DNMT1 promoter was

generated by restriction digestion. Briefly, human DNMT1 promoter regions (−892∼+349) were amplified by polymerase chain reaction (PCR) using the following primers, which add Mlu I or Bgl II restriction sites at the 5′ end: forward 5′-CGACGCGTTAGGATTA-CAGGTGTGTGTC-3'; reverse 5′-GGAAGATCTCCCTGAGTCCGTGTT CC-3'. The PCR products were double-digested with Mlu I and Bgl II and inserted into the Mlu I and Bgl II restriction sites of the PGL3-Basic vector (Promega). For detecting p53 activation, 10 µg of p53 luciferase reporter plasmids and pSV-β-galactosidase plasmids were co-transfected into SMCs. 24 h post-transfection, cells were seeded on soft vs. stiff PA gels and cultured for 24 h. Luciferase activity was measured using the luciferase assay system (Beyotime) and normalized to the β-galactosidase activity assessed using o-nitrophenyl-β-D-galactopyranoside (Amresco). HeLa cells were used for plasmids transfection to ensure high transfection efficiency in the followed experiments. For detecting DNMT1 transcriptional activity, cells were co-transfected with DNMT1-luciferase reporter plasmids and pSV-β-galactosidase plasmids. 8 h post-transfection, cells were treated with DDR1-IN-1 at 10 µmol/L for 3 h, and 24 h post-transfection, the luciferase activity was measured.

2.4. Polyacrylamide (PA) gel preparation

PA gels were prepared as previously described [28]. Briefly, 40% w/v acrylamide and 2% w/v bis-acrylamide (Bio-Rad) stock solutions were mixed and supplemented with N, N, N9, N9-tetramethylethylenediamine (TEMED) and ammonium persulfate to initiate gel polymerization. Gels with different stiffness were obtained by varying the final concentrations of acrylamide (4% and 8%) and bis-acrylamide (0.3% and 0.264%) for the corresponding elastic moduli of ∼3.24 and ∼19.66 kPa, that were selected to mimic soft and stiff substrates, respectively, according to published literatures [28,29]. The stiffness of PA gel also fits into the range of elastic moduli (2.30 kPa–24.9 kPa) of atherosclerotic lesions in human carotid arteries measured in our earlier work [2]. A 50-70 µm-thick gel was cast, and the thickness was confirmed by imaging of embedded fluorescent beads in the gel with confocal microscopy. To cross-link matrix proteins onto the gel surfaces, hetero-bifunctional crosslinker sulfo-SANPAH (Pierce) at 0.5 mg/ml was added on top of the gels and the surfaces were activated by UV (365 nm) exposure. Collagen type I (Corning) at 0.1 mg/ml or fibronectin (Corning) at 0.05 mg/ml were coated on the activated gel surfaces. The elastic moduli of PA gels were measured by nanoindentation. To block the interaction between collagen and DDR1, blocking protein DDR1: Fc or control IgG were added into 0.1 mg/ml collagen in PBS to a final concentration of 10 µg/ml [30]. The mixture was incubated at 4 °C for 4 h and was then used for gel coating.

2.5. Measurement of material stiffness with nanoindentation

The elastic moduli of tissue, cell and matrix were measured by nanoindentation. We used the ferrule-top nanoindenter setup together with the PIUMA controller/drive (Optics11, Amsterdam; The Netherlands) [31]. Samples were measured as previously described [2]. For tissue measurement, probes with the spring constants from 0.46 to 8.1 N/m and the spherical tips with the radius from 30 to 81 µm were used. For cell and matrix measurement, a probe with a 0.049 N/m spring constant and a spherical tip with a radius of 9 µm was used. During indentation, the tip was kept in liquid environment and was brought into contact with the cell surface or ECM under monitoring with a microscope to ensure accurate measurement. The load-indentation and load-time data were recorded. The indents were depth controlled (10 µm) and the loading and unloading period was set to be 2 s. Based on the load-displacement curves, the reduced Young's modulus (RedYM) was calculated using the Hertz spherical indentation model. For each specimen, the mean Young's modulus was generated from 20 to 30 single measurements in three independent tests. For arterial tissue analysis, 20 to 30 measurements were made on each tissue specimen. The Young's

modulus of the cell-adjacent-matrix was measured by placing the tip onto the gel surface appropriate 10 µm from the cell boundary.

2.6. Atomic force microscope (AFM) assay

The AFM assay was performed as described previously [32]. Briefly, cells with indicated treatments were grown on soft or stiff gels in culture dishes for 24 h. The cantilever tip (MLCT; Bruker AFM Probes) was coated with 500 µg/ml collagen type I (Corning) by incubation for 2 h at 37 °C, and was then blocked by 1% bovine serum albumin (BSA) for 1 h at 37 °C. The culture dishes were placed on the AFM stage. Measurements were acquired with the followed parameters: cantilever approach velocity 1 µm/s; contact duration 0 ms; compression force 300 pN; and retraction velocity 1 µm/s. The collagen-captured cantilever was driven by a piezoelectric translator repeatedly to make approach-contact-retract events on cell surface. The single-bond adhesion and dissociation between cantilever tip and cell membrane were recorded as a peak in the force-displacement curves. The rupture force of the cell membrane DDR1-collagen bond was obtained from the deflection of the cantilever [32]. 3 or 6 independent experiments were performed with different cantilevers which have the same size (320 µm long, 22 µm wide). In one experiment, 10 cells in each group were measured by contacting with cantilever tip. 50–60 approach-contact-retract repeats were performed on each region to obtain adhesion events and single-bond rupture force. The adhesion probability was calculated according to the ratio of adhesion events to all contact events in one experiment.

2.7. SMC-macrophage coculture

We established a coculture model for assaying attraction of RAW264.7 macrophages towards SMCs cultured on gels. Briefly, PA gel was prepared on glass slide, which was placed on the bottom of a 35-mm culture dish. SMCs were seeded on the PA gel and maintained in F-12 Ham supplemented with 10% FBS. A transwell insert (#353097, FALCON) with microporous membrane (with 8 µm pores) was incorporated into the culture dish, avoiding directly contacting with the gel or SMCs. Macrophages were then plated on the upper side of microporous membrane and maintained in DMEM without FBS. After incubation for 48 h, the microporous membrane was collected, and the macrophages on the upper side were removed using sterile cotton gauze. Macrophages migrated to the lower side of the membrane were fixed by 4% paraformaldehyde and stained with crystal violet solution. The migrated cells were counted under microscope.

2.8. RNA isolation and real-time reverse transcription (RT)-PCR

RNAs were extracted from tissues and cells using TRIzol reagent (Invitrogen) according to the manufacturer's instructions. The isolated RNAs were reversed-transcribed into complementary DNA with M-MLV RT system (Invitrogen). Real-time PCR was performed with Hieff® qPCR SYBR® Green Master Mix (YEASEN). The results were analyzed and calculated by 2-ΔΔCt method. Gene expression was normalized against GAPDH.

2.9. Western blot assay

Cells and tissues were lysed in RIPA buffer (150 mmol/L sodium chloride, 50 mmol/L Tris-HCl (pH 7.5), 1% Triton X-100, 1% sodium deoxycholate, 0.1% SDS, 2 mmol/L EDTA) containing PMSF, proteinase inhibitors and phosphatase inhibitors. Protein concentration was determined with the Bicinchoninic Acid (BCA) assay by Pierce™ BCA Protein Assay Kit (Thermo). Equal amounts of proteins were separated on sodium dodecyl sulphate-polyacrylamide gel electrophoresis (SDS-PAGE), transferred to nitrocellulose membranes, blocked with 5% skim milk in Tris-buffered saline (TBS) containing 0.1% Tween 20 (TBST), and incubated with the indicated primary antibodies over night at 4 °C.

After incubation with donkey anti-rabbit/-mouse IgG (H&L) antibody IRDye 800/700 Conjugated (Rockland) or HRP-conjugated secondary antibodies, the blots were visualized by Odyssey infrared imaging system (LI-COR Biosciences) or Molecular Imager ChemiDoc XRS + System (Bio-Rad).

2.10. Cell fractionation

SMCs were washed with PBS and lysed with buffer A (10 mmol/L Tris PH7.5, 1.5 mmol/L $MgCl_2$, 10 mmol/L KCl, 0.5% NP-40), followed by centrifugation at 7000 rpm for 5 min. The supernatants were collected (containing cytoplasmic and membrane proteins). The precipitations were re-suspended in buffer B (20 mmol/L Tris pH 7.5, 1.5 mmol/L $MgCl_2$, 420 mmol/L NaCl, 10% Glycerol, 0.2 mmol/L EGTA) and centrifuged to get the nuclear fractions.

2.11. Chromatin immunoprecipitation

SMCs were cultured either on soft or stiff substrates for 24 h. The cells were harvested and then washed once with PBS (room temperature), crosslinked with 1% formaldehyde in PBS for 10 min, rinsed twice with ice-cold PBS and resuspended with 300 μl of lysis bufer (1% SDS, 5 mmol/L EDTA, 50 mmol/L Tris-HCl (pH 8.1), and protease inhibitors), incubated on ice for 10 min, and sonicated for 3 times at 12 s each. 10% aliquot was saved as an input. The lysate was 1:10 diluted in dilution buffer (1% Triton X-100, 2 mmol/L EDTA, 150 mmol/L NaCl, 20 mmol/L Tris-HCl (pH 8.1), and protease inhibitors), and was incubated with antibody against DNMT1 for 6 h or overnight at 4 °C and then with 30 μl of protein A-G sepharose beads for another 2 h. The sepharose beads were washed sequentially with buffer TSE I (0.1% SDS, 1% Triton X-100, 2 mmol/L EDTA, 20 mmol/L Tris-HCl, pH 8.1, 150 mmol/L NaCl), buffer TSE II (0.1% SDS, 1% Triton X-100, 2 mmol/L EDTA, 20 mmol/L Tris. HCl, pH 8.1, 500 mmol/L NaCl), buffer III (0.25 mol/L LiCl, 1% NP-40, 1% deoxycholate, 1 mmol/L EDTA, 10 mmol/L Tris. HCl, pH 8.1), and TE buffer. Crosslinks were reversed at 65 °C overnight. DNA was extracted with DNA Pure-Spin Kit (Vigorous), and subjected for PCR amplification.

2.12. Immunofluorescence and immunohistochemistry

For immunofluorescence assay in cultured cells, SMCs grown on PA gels were fixed with 4% paraformaldehyde for 15 min and permeabilized with 0.25% Triton X-100 for 10 min. After blocked with 5% BSA, cells were incubated with primary antibody against DDR1, p53 or Rab 5A over night at 4 °C. After incubation with second antibody, cells were mounted with mounting medium containing DAPI and visualized by confocal-microscopy (Leica DMI6000B, Leica TCS SP8 stimulated emission depletion (STED)). The acquisition mode on the same microscope setup could be switched between confocal (diffraction limited resolution, excitation lasers only) or STED (with the depletion beam additionally switched on), as described previously [33]. For STED imaging, the dyes STAR ORANGE and STAR RED were applied for their high photostability. For quantification of p53 localization, the regions of cell nucleus or cytoplasm were manually determined, and fluorescence intensities were measured using ImageJ. For three-dimensional reconstruction of DDR1 clusters, cells were scanned layer-by-layer along Z axis and the images were reconstructed with Leica TCS SP8 confocal-microscopy. Immunofluorescence of human specimen and mice vessel were similar to that in cultured cells. The samples were fixed over night with 4% paraformaldehyde and were then dehydrated with ethanol. The paraffin sections were prepared before staining. Antigen retrieval was performed in a steamer. Ratio of p-DDR1 positive cells to SMA-positive cells was quantified using Image J software. For immunohistochemistry staining, DAB (Vector Laboratories) and Hematoxylin counterstaining (Sigma) were used.

2.13. Human specimen

Internal mammary arteries from patients (#1, male, age 59; #2, male, age 66; #3, male, age 69) undergoing coronary artery bypass grafting and atherosclerotic plaque from patients (#4, male, age 60; #5, male, age 64; #6, male, age 65; #7 male, age 47; #8, male, age 59) undergoing carotid endarterectomy were obtained from Peking University People's Hospital with the agreement of the patients and approved by the Peking University People's Hospital Medical Ethics Committee (2015PHB024). The patients undergoing carotid endarterectomy were examined with color Doppler ultrasonography or computed tomographic angiography and were diagnosed severe (>70%) carotid stenosis. Immunohistochemistry, immunofluorescence, and measurement of stiffness in human specimen were carried out in accordance with the approved guidelines. For stiffness measurement, patients' plaques were divided into three parts according to the degree of calcification. The elastic moduli were measured by nanoindentation.

2.14. Experimental animal models

All animal studies were performed in accordance with the guidelines of the Animal Care and Use Committee of Peking University and approved by the Ethics Committee of Peking University Health Science Center (LA2018155). Dnmt1$^{flox/flox}$ (B6.129S4-Dnmt1^{tm2Jae}/Mmucd, MMRRC, stock number 014114-UCD, Dnmt1$^{fl/fl}$) mice were mated with transgenic mice expressing CreER^{T2} under the control of the mouse smooth muscle myosin, heavy polypeptide 11, Myh11 promoter (Myh11-CreER^{T2}, Jackson Laboratories, stock number 019079) to generate mice with Dnmt1 (Dnmt1^{WT}) or without Dnmt1 (Dnmt1^{sKO}) expression in vSMCs. In the Myh11-CreER^{T2} mice, the bacterial artificial chromosomes (BAC) transgene was inserted on the Y Chromosome and hence only male mice could express the Cre recombinase. Male mice were subjected to tamoxifen (dissolved in corn oil) intraperitoneal injection with 40 mg/kg every day for 5 days. Three weeks after injection, mice were sacrificed and the efficiency of Dnmt1 depletion was verified by Western blot.

In a model of acute vascular injury, 12-week-old C57/BL6 male mice were randomly divided into 4 groups: the aortic injury groups with treatment of either DDR1-IN-1 or the control solvent, the sham groups with treatment of either DDR1-IN-1 or the control solvent. Mice in the DDR1-IN-1 groups were intraperitoneally injected daily with 0.2 mg/kg DDR1-IN-1 in saline for 5 days. Mice in the control solvent groups were injected with equal amount of DMSO in saline. After injections for 5 days, the animals were anaesthetized and subjected to a laparotomy for exposure of infrarenal abdominal aortas. Sterile cotton gauze soaked in 0.5 moL/L $CaCl_2$ or saline was applied to the abdominal aortas and then incubated with the aortas for 10 min to induce acute aortic injury. 7 days after the operation, mice were sacrificed and the $CaCl_2$ or saline incubated abdominal aortas (~1 cm in length) were harvested for analyses.

In a model of chronic kidney failure, 12-week-old C57/BL6 male mice were divided into 4 groups: chow diet with DMSO, adenine diet with DMSO, adenine diet with DDR1-IN-1 (0.2 mg/kg), or adenine diet with both DDR1-IN-1 (0.2 mg/kg) and 5-Aza (0.2 mg/kg). The inhibitors or control solvents were delivered via intraperitoneal injection. All the groups were given 6-week distinct diets (chow vs. adenine (0.2% adenine)). Injections were conducted every 3 days during the distinct diet. After 6 weeks feeding, mice were subjected to functional and morphological analyses.

2.15. Characterization of calcium deposition by Alizarin Red S staining

Frozen/paraffin sections were washed with ultra-pure H_2O, fixed with 4% formaldehyde for 10 min, washed with H_2O and then incubated with 0.2% Alizarin Red S in water overnight at 37 °C, followed by washed with 0.2% acetic acid. Positively stained tissue displayed a reddish/purple color.

2.16. RNA-sequencing and expression profiling

Aortas from Dnmt1^{WT} and Dnmt1^{sKO} mice were collected and the endothelia and adventitia were removed. Total RNAs were extracted with TRIzol Reagent. High-throughput sequencing was performed at the Beijing Genomics Institute (BGI), China. Data analysis were performed as previously described [34,35]. The HISAT and Bowtie2 software were used to map the clean data to the mouse reference genome (GCF_000001635.26_GRCm38.p6). The read length was PE (paired end reads) 150. Gene expression level was quantified by RSEM (http://dewe ylab.biostat.wisc.edu/rsem/rsem-calculate-expression.html). The threshold of differentially expressed genes (DEGs) was set to be |log$_2$ Fold change | ≥ 0.5 and an adjust P value ≤ 0.05. DEGs were analyzed using DEseq2 (http://www.bioconductor.org/packages/release/bioc/h tml/DESeq2.html). Gene Ontology (GO) and Kyoto Encyclopedia of Genes and Genomes (KEGG) enrichment analyses were carried out with the DAVID functional annotation tools (http://www.david.niaid.nih. gov). Gene Set Enrichment Analysis (GSEA) was performed using the GSEA software (https://www.gsea-msigdb.org/gsea/index.jsp).

2.17. Ultrasound imaging in mouse

A Vevo 3100 LAZR ultrasound system (FUJIFILM Visual Sonics, Canada) was used for vascular ultrasound imaging in mouse. Dnmt1^{WT} and Dnmt1^{sKO} mice were anaesthetized by 1.5–2% isoflurane and placed on the platform that carries electrocardiogram (ECG) electrodes. Heart rate and ECG were recorded. Luminal diameter and vessel wall thickness were measured by M-mode ultrasonography at aortic arch and carotid artery, and the pulse wave velocity (PWV) was measured by B-mode and Doppler-mode. Briefly, in a long-axis view of carotid artery, the vascular pulse-wave Doppler tracing was recorded at the position of carotid bifurcation (position 1). The time from the onset of the QRS to the onset of the Doppler waveform was measured (T1). The position in the distal area from the carotid bifurcation was selected and the pulse-wave Doppler tracing was recorded (position 2). The time from the onset of the QRS to the onset of the Doppler waveform was measured as T2. The distance between position1 and position2 was measured (L). PWV is calculated as: L/(T1-T2) (m/s). The values for T1 and T2 were the average of three measurements.

2.18. Measurement of isometric force by wire myograph

Wire myograph experiment was performed as previously described [36]. Mice were euthanized and the thoracic aortas were isolated and placed in oxygenated ice-cold Krebs-Henseleit solution. The adventitia and endothelium were removed. The aortas were cut into 2 mm-long aortic ring segments and mounted to a Multi Myograph System (Danish Myo Technology, Aarhus, Denmark). 3 mN pretension was reached and set as the baseline of vasocontraction force. Isometric tension envoked by KCl and Phenylephrine Hydrochloride (Phe) were measured. In brief, 60 mmol/L KCl was administered to verify the vessels' contractile ability and provide a setpoint of maximum value for contraction force. KCl was washed out with Krebs-Henseleit solution. The contraction force after cumulative concentrations of KCl (10–80 mmol/L) or Phe (10^{-9}–10^{-4} mol/L) were measured. After maximal contraction, we examined vasorelaxant potential using sodium nitroprusside (SNP) in increasing concentrations (10^{-9}–10^{-4} mol/L).

2.19. Statistical analysis

Data are presented as mean ± SEM of the mean from at least three independent experiments as indicated. For in-vitro experiments, as each experimental data set is an average of a large number of cultured cells, we assumed the data was normally distributed based on the central limit theorem. For in-vivo experiments, the n value represents independent repeats or the numbers of animals. All analysis was performed using GraphPad Prism version 8.3.0. Normality of data distribution was tested with a D'Agostino-Pearson, Aderson-Darling, Kolmogorov-Smirnov or Shapiro-Wilk test. For normally distributed data, differences between treatment groups were determined using paired or unpaired t-test for two groups of data and one-way or two-way ANOVA for multiple groups of data. Statistical significance among multiple groups was determined by post hoc analysis (Newman-Keuls honestly significant difference test). Nonparametric tests were used when data were not normally distributed, the Kruskal-Wallis test was conducted to test statistical significance for experiments with ≥3 groups followed by Dunn's post-hoc test, and the Mann-Whitney test was used to examine statistical significance between 2 groups. Values of P < 0.05 were considered statistically significant.

3. Results

3.1. Substrate stiffness activates DDR1 in a collagen-independent manner

To investigate the matrix stiffness-induced DDR1 activation, human umbilical artery SMCs were cultured for 24 h on collagen type I-coated PA substrates whose stiffness was adjusted to fit into the range of physiologically and pathophysiologically relevant conditions corresponding to the elastic moduli of healthy and diseased vessel walls (Fig. S1) [2,28,29]. DDR1 activation is accompanied by receptor phosphorylation at Try792 [24], a site that could be constantly phosphorylated upon treatment of SMCs with collagen type I (Fig. S2). Not surprisingly, substrate stiffness increased Try792 phosphorylation of DDR1 (p-DDR1), but not the basal DDR1 expression, in cells on collagen-coated gels (Fig. 1A). DDR1 is known to bind various types of collagens [20]. Application of a DDR1 blocking molecule (recombinant protein DDR1: Fc that disrupts the DDR1-collagens interactions [30] reduced the capacity of DDR1 phosphorylation to collagen type I, whereas a control immunoglobulin had no such effect (Fig. S3). However, DDR1: Fc did not interfere with the stiffness-induced DDR1 phosphorylation (Fig. 1B), suggestive of an independence of mechanical activation of DDR1 on its natural ligands. To further test this independence, collagen type I was replaced with fibronectin, an ECM protein that would not activate DDR1. Compared with cells on fibronectin-coated soft substrates, a remarkable increase in p-DDR1 on stiff substrates was observed (Fig. 1C), similar to the stiffness-induced p-DDR1 increase on collagen-coated gels. DDR1 activation is accompanied by receptor oligomerization and internalization [37,38]. STED super-resolution microscopy and the three-dimensional reconstruction of confocal images indicated that substrate stiffness induced aggregation and oligomerization of DDR1 into a clustered and punctate distribution in the cytoplasm (Figs. 1D and S4). In addition, in cells on stiff substrates, the DDR1 clusters were surrounded by Rab5A signals that indicate early endosomes [39,40], demonstrative of DDR1 internalization. Treatment of the cells with a potent and selective DDR1 receptor tyrosine kinase inhibitor, DDR1-IN-1, diminished the stiffness-induced oligomerization and internalization of DDR1 (Fig. 1D).

To confirm DDR1 activation by matrix stiffness, we performed AFM assay based on the speculation that receptor activation leads to enhanced interaction with its ligands [41]. Direct measurements of molecular adhesion and bond rupture forces between the ligand-captured AFM probe and the surfaces of SMCs on fibronectin-coated gels were conducted (Fig. 1E). First of all, the specificity of collagen-capture of the AFM probe was confirmed by comparing collagen with BSA coating, and the latter displayed a significantly reduced adhesion probability and adhesion force with the cell membrane (Fig. 1F). This confirmed that the adhesion events between collagen and DDR1 in the cell membrane were specific. Then we found that the adhesion probability between the probe and the cell membrane was greatly promoted to 32.43 ± 1.40% in cells on stiff gels, as compared with 18.28 ± 2.31% on soft gels (Figs. 1G and S5). The increased adhesion probability might be attributable to the
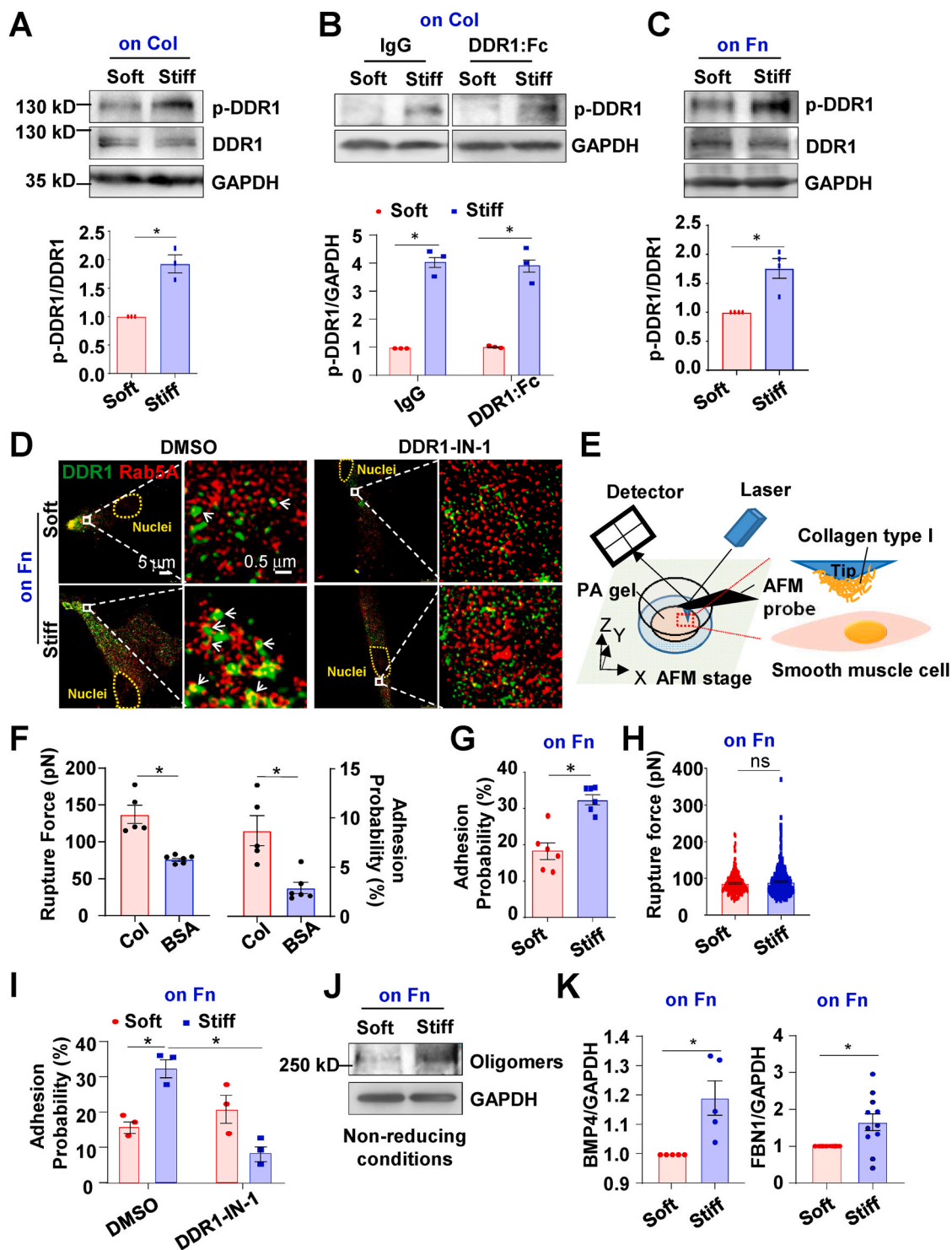
Fig. 1. Substrate stiffness-induced DDR1 activation is independent of collagen binding. *(A)* to *(C)* Western blot assay to determine phosphorylation of DDR1 at tyrosine 792 (p-DDR1) and the total DDR1 expression. GAPDH served as an internal control. Shown are representative blots from at least 3 independent experiments. Semi-quantification (in the lower panels) of indicated protein was performed by using the ImageJ software based on the analysis of the gray band intensity. *(A)* The p-DDR1 and total DDR1 levels in SMCs cultured for 24 h on collagen type I (Col) coated-polyacrylamide (PA) gels with a stiffness of 2 (soft) or 20 (stiff) kPa. *(B)* The p-DDR1 levels in SMCs grown on Col-coated gels for 24 h in the presence of the DDR1: Fc peptides. *(C)* The p-DDR1 and total DDR1 levels in SMCs cultured for 24 h on fibronectin (Fn)-coated PA gels. *(D)* Representative stimulated emission depletion microscopy (STED) images of DDR1 and Rab5A immunofluorescence in SMCs on Fn-coated gels. Cells were either pretreated with DDR1-IN-1 or DMSO. *(E)* Schematic diagram illustrating measuring the interaction between the collagen and the surfaces of SMCs by atomic force microscopy (AFM). *(F)* AFM to determine the adhesion probability and rupture forces between the Col- or BSA-coated probe and the cell surface. Each dot represents one cell. *(G)* and *(H)* AFM to determine the adhesion probability and rupture forces between the DDR1 ligand (Col) and the cell surface. In *(G)*, each dot represents an independent experiment, and in *(H)*, each dot represents the rupture force of a single bond between Col and the cell surface. *(I)* AFM to determine the adhesion probability in cells that were pretreated with DDR1-IN-1 or DMSO and cultured on Fn-coated gels. Each dot represents an independent experiment. *(J)* Western blot assay to determine DDR1 and GAPDH in cell lysates prepared using a non-reducing condition. *(K)* Quantitative RT-PCR to determine the expressions of DDR1 targeted genes in SMCs on Fn-coated gels. Each dot represents an independent experiment. *$P < 0.05$ vs. the indicated group.

stiffness-induced DDR1 clustering. In contrast, the rupture forces between the probe and the cell surface on soft vs. stiff gels were quite similar (Figs. 1H and S5), suggesting no conformational alternation of DDR1 caused by substrate stiffness. The increase in adhesion probability in cells on stiff gels could be completed abrogated by treatment of the cells with DDR–IN–1 at 10 µmol/L for 3 h (Fig. 1I), validating the role of DDR1 in mediating the interaction between collagen and the cell. In agreement with the AFM findings, analysis of DDR1 expression in cell lysates prepared using a non-reducing condition indicated increased DDR1 oligomer formation in cells on stiff vs. soft gels (Fig. 1J). Moreover, quantitative RT-PCR analysis revealed that the expression of DDR1 target genes, including BMP4 and FBN1 [42], were significantly upregulated in cells on fibronectin-coated stiff gels vs. that on soft (Fig. 1K). Taken together, the data demonstrate that substrate stiffness activates DDR1 and the activation can be independent of collagen binding.

3.2. DDR1 is activated in calcified atherosclerotic lesions of human carotid arteries

To determine whether the stiffness of vascular wall and DDR1 activation are related in vivo, carotid endarterectomy specimens from patients with carotid occlusive diseases were obtained to study DDR1 expression and phosphorylation in the atherosclerotic lesions where ECM usually becomes stiffer than the adjacent normal areas. Each specimen was divided into three regions according to the degree of calcification (Fig. S6), and elastic moduli were measured by nanoindentation (Fig. S7). The elastic modulus increased to ~7.38 kPa in proximal areas compared with that in distal areas and up to ~21.82 kPa in plaque areas (Fig. 2A). Immunohistochemistry revealed markedly elevated p-DDR1 in plaque area compared with that in the softer proximal and distal areas, whereas the basal DDR1 expression levels among the distinct areas were comparable (Fig. 2B). DDR1 phosphorylation was also detected by immunofluorescence staining. Compared with that in distal areas, ratios of p-DDR1-positive vSMCs were much greater in proximal and reached to the greatest in plaque areas (Fig. 2C). Indeed, compared with that in non-diseased normal internal mammary arteries, ratios of p-DDR1-positive vSMC and p-DDR1 levels also increased in plaque areas, but the basal DDR1 expression levels remained similar (Fig. 2D and E). These results demonstrate DDR1 activation in arterial stiffening. Intriguingly, we found that in plaque or proximal areas, the level of 5-mC was remarkably lower than that in distal (Fig. S8), implying potential epigenetic outcomes involved in arterial stiffening.

3.3. DDR1 mediates substrate stiffness-induced downregulation of DNMT1 expression

We then tested our hypothesis that DDR1 activation leads to dysregulation of DNMT1, the enzyme that mediates the 5-C/5-mC conversion. Human umbilical artery SMCs were cultured for 24 h on collagen type I-coated PA gels with variable stiffness (2–40 kPa) and a gradually decreased expression of DNMT1 accompanied by stiffness increasing was observed (Fig. 3A). Indeed, SMCs grown on plastic culture dishes that had been pre-coated with collagen I solutions at indicated concentrations (from 0 to 150 µg/mL) also exhibited a dose-dependent reduction of DNMT1 expression (Fig. 3B), suggesting that collagen binding may initiate the signaling linked to DNMT1 inhibition. To determine the role of DDR1 in mediating the stiffness-regulation of DNMT1 expression, cells were pretreated with DDR1-IN-1 (10 µmol/L) or transfected with siRNAs that recognize DDR1 and were subsequently cultured on the collagen-coated gel substrates. As expected, substrate stiffness down-regulated the DNMT1 expression, while the downregulation could be abolished either by DDR1-IN-1 treatment or by DDR1-knockdown (Fig. 3C and D). We wondered whether the stiffness-activated DDR1-to-DNMT1 signaling is dependent on collagen. To address this question, the expressions of DNMT1 in cells on collagen- or fibronectin-coated gel substrates were compared. In agreement with the

observations on collagen-coated gels, the DNMT1 levels on fibronectin-coated gels were also regulated by stiffness (Fig. 3E). Knockdown of DDR1 reversed the stiffness-provoked DNMT1 inhibition in cells on fibronectin-coated gels (Fig. 3F). Taken together, these results indicated that DDR1 mediates the DNMT1 expression regulation by substrate stiffness and the effect is independent of collagen.

3.4. The ERK-p53 pathway is involved in the DDR1-mediated DNMT1 regulation by matrix stiffness

Next, we explored the mechanism by which DDR1 regulates DNMT1 expression. Luciferase reporter plasmids driven by the putative promoter regions of DNMT1 (−892~+349) were constructed (Fig. S9A) and transfected into HeLa cells to ensure higher transfection efficiency. Compared with the control transfection that characterizes a basal luciferase activity, transfection with the DNMT1-promoter-driven reporters markedly increased the luciferase activity; the increase was further enhanced upon treatment with DDR1-IN-1 (Fig. S9B). This result revealed that DDR1 inhibits the DNMT1 expression at the transcriptional level. Analysis for transcription factor binding sites within the DNMT1 promoter using the PROMO database predicted two p53 binding sites (Fig. 4A). To determine the role of p53 in regulating DNMT1 expression, cells were pre-treated with p53 inhibitor Pifithrin-α (PFTα) at 10 µmol/L and grown on gel substrates. Western blot assay showed that substrate stiffness decreased DNMT1 expression while activated p53 phosphorylation at serine 15 (Ser15) (Fig. 4B and C), the latter is positively related to p53 activation [43], and that treatment of cells with PFTα eliminated the stiffness-elicited inhibitory effect on DNMT1 expression (Fig. 4C). To confirm the activation of p53 by stiffness, luciferase activity assay was carried out in the on-gel growing SMCs that have been transfected with luciferase reporter plasmids driven by p53 responsible elements. We observed an increased luciferase activity of p53 on stiff gels vs. that on soft (Fig. 4D). Verification of p53 activation was provided by cell fractionation assay that indicated a cytoplasmic-to-nuclear translocation of p53 on stiff gels (Fig. 4E). Furthermore, chromatin immunoprecipitation experiment was performed to assess the binding of p53 to the promoter regions of DNMT1 in vSMCs grown on gel substrates. The results demonstrated higher enrichment of p53 within the DNMT1 promoter in cells on stiff gels than that on soft gels (Fig. 4F).

To investigate the signaling pathways from DDR1 to p53, cells were pre-treated with DDR1-IN-1, cultured on gel substrates, and then the cellular distributions of p53 were determined by immunofluorescence. The nuclear translocation of p53 in cells on stiff gels was restricted by treatment of the cells with DDR–IN–1 (Fig. 4G). Further study showed that the matrix stiffness-induced p53 phosphorylation could be attenuated by DDR1 inhibition (Fig. 4H) or by DDR1 knockdown (Fig. S10). We sought to elucidate how DDR1 regulates p53 activation. Ser15 phosphorylation of p53 is catalyzed by kinases including ERK1/2 [44], which can be phosphorylated by collagen-induced activation of DDR1 [45,46]. We tested whether ERK1/2 are involved in the stiffness-initiated DDR1-to-p53 signaling in SMCs. The phosphorylation, but not the total level, of ERK1/2 was found to be induced by culturing on stiff substrates (Figs. 4H and S11). The induction was suppressed by treatment with DDR1-IN-1or with DDR1-specific siRNA (Figs. 4H and S11). To test the role of ERK1/2 in mediating p53 activation, cells were treated with PD98059 at 50 nmol/L to block the MAP kinse-ERK kinase (MEK)-mediated activation of ERKs. The stiffness-activated phosphorylation of p53 was suppressed by treatment of the cells with PD98059 (Fig. 4I). In summary, these data demonstrate that ERK1/2 are downstream of DDR1 to regulate p53 phosphorylation in response to matrix stiffness, and that the ERK-p53 pathway mediates the DDR1 to DNMT1 signaling in SMCs.
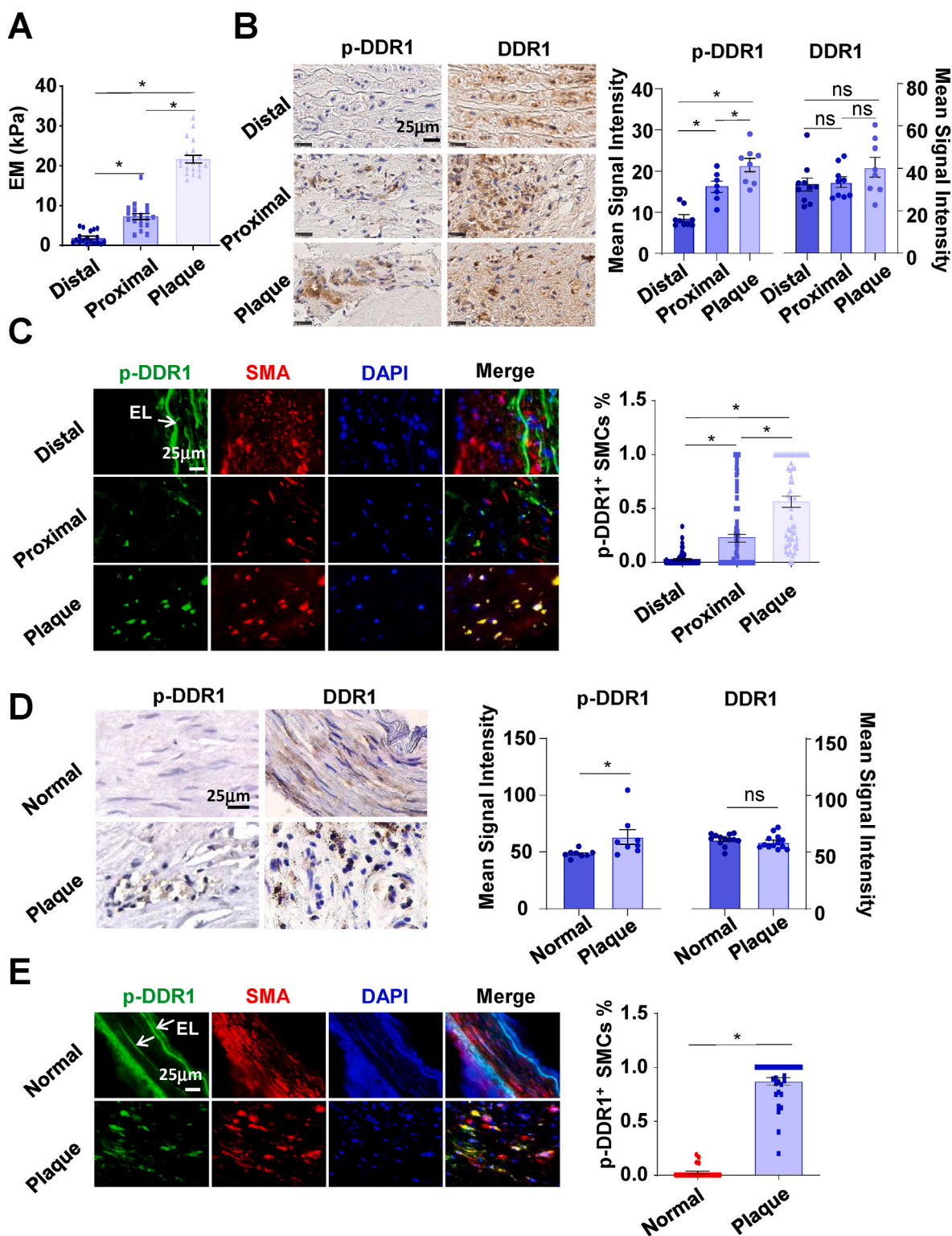
Fig. 2. The phosphorylation level, but not the total level, of DDR1 is increased in calcified atherosclerotic plaques.
(A) The Elastic moduli (EM) of the distal, proximal, and plaque regions in human carotid endarterectomy specimens measured by nanoindentation. Each dot means one measurement. Each group contains 20 to 30 single measurements at different points. *(B)* Representative immunohistochemistry staining and the quantification of p-DDR1 and DDR1 in the carotid endarterectomy specimens. *(C)* Representative immunofluorescent images of p-DDR1 and SMA in distinct regions of the carotid endarterectomy specimens. *(D)* Representative immunohistochemistry staining and the quantification of p-DDR1 and DDR1 in the normal and plaque specimens. *(E)* Representative immunofluorescent images of p-DDR1 and SMA in the carotid endarterectomy specimens (plaque) and the control internal mammary artery (normal). For quantification of *(C)* and *(E)*, the ratio was obtained by calculating the percentage of p-DDR1-positive cells in SMCs (SMA-positive cells). One dot represents a value calculated from one field. $*P < 0.05$ vs. the indicated group.
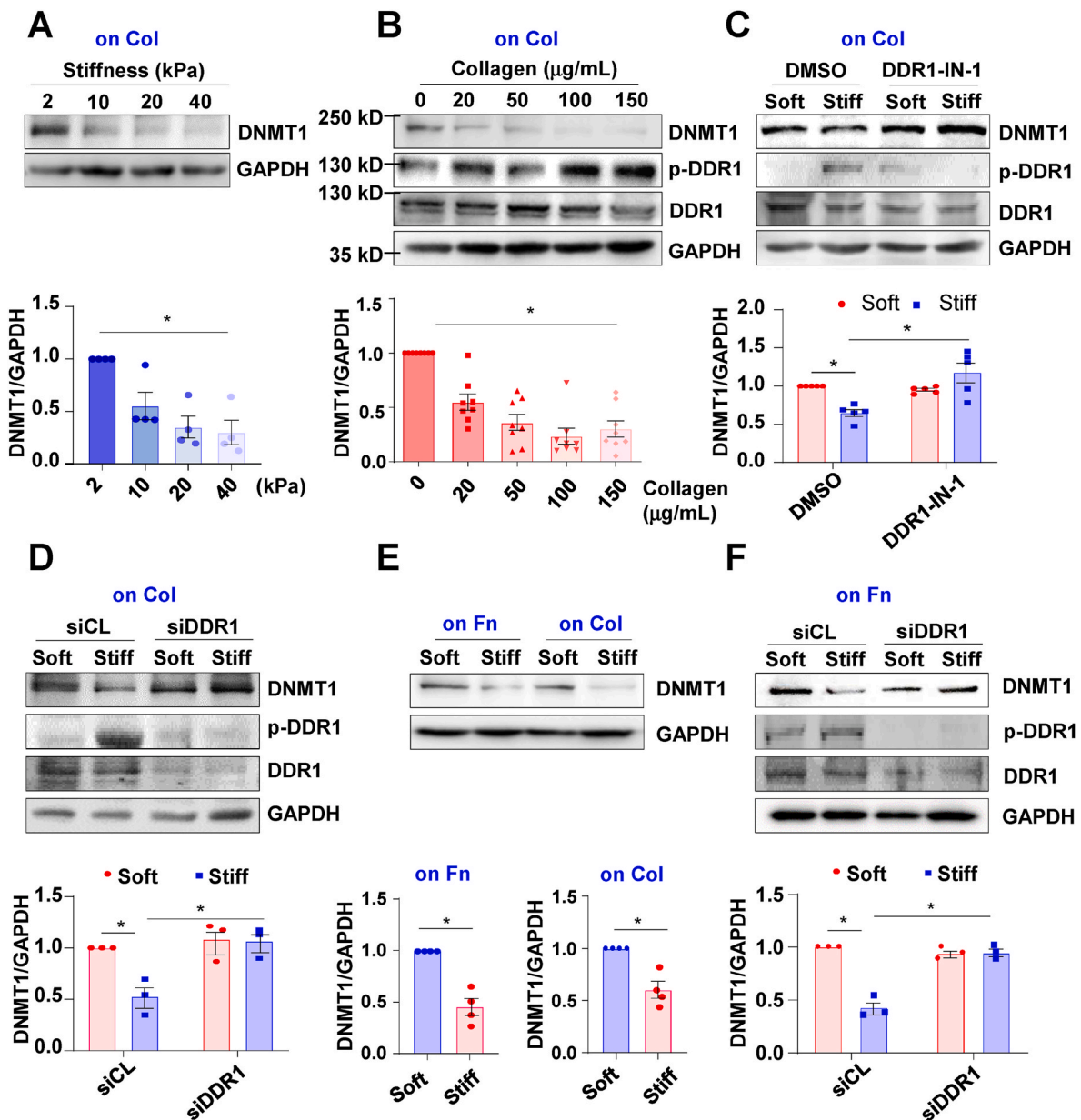
Fig. 3. DDR1 mediates substrate stiffness-induced downregulation of DNMT1 expression. Western blot assay to determine the expressions of DNMT1, p-DDR1, DDR1 and the internal control GAPDH in vSMCs with the indicated treatments. Shown are representative blots from at least 3 independent experiments. Semi-quantification of indicated proteins were performed by using the ImageJ software based on the analysis of the gray band intensity. One dot represents a biological repeat. *(A)* The protein level of DNMT1 in SMCs cultured for 24 h on collagen type I (Col) coated-gels with the indicated stiffness. *(B)* The protein level of DNMT1 in SMCs grown in dishes that have been pre-coated with Col at variable concentrations. *(C)* and *(D)* The expressions of DNMT1, p-DDR1, and DDR1 were determined in SMCs, which were either pretreated with DDR1-IN-1 or the control reagent (DMSO) *(C)* or transfected with siRNA targeting DDR1 (siDDR1) or scrambled siRNA (siCL) *(D)*. *(E)* The expression of DNMT1 was determined in SMCs grown on fibronectin (Fn)- or Col-coated gels. *(F)* The expressions of DNMT1, p-DDR1, and DDR1 were determined in SMCs transfected with siDDR1 or siCL on Fn-coated gels. *$P < 0.05$ vs. the indicated group.

3.5. vSMC-specific depletion of Dnmt1 results in arterial stiffening and vascular dysfunction

To investigate the functional relevance of DDR1-DNMT1 axis in vivo, SMC-specific Dnmt1 knockout mice Dnmt1^{sKO} (Dnmt1$^{f/f}$, Myh11-CreER^{T2+}) and littermate control Dnmt1^{WT} (Dnmt1$^{f/f}$, Myh11-CreER^{T2-}) were generated followed by tamoxifen injection. The efficiency of Dnmt1 depletion was tested by Western blot and immunofluorescence (Fig. 5A and B). No significant difference of body weight and blood pressure were detected between Dnmt1^{sKO} and Dnmt1^{WT} (Fig. S12). Dnmt1 deficiency led to a significant increase in carotid PWV (Fig. 5C), suggestive of arterial stiffening. This result is in line with our previous

finding that pharmacological inhibition of Dnmt1 in mice increased the elastic modulus of the vessel wall [2]. Alizarin red S staining assay revealed calcium deposits in the Dnmt1 deficient vessels (Fig. 5D), indicative of calcification as a potential cellular mechanism of arterial stiffening. Because studies have indicated an importance of inflammation in the pathogenesis of arterial stiffness [9,10], we measured the level of proinflammatory cytokine MCP1 in vessel wall and found that the arteries from Dnmt1^{sKO} mice displayed profound MCP1 expression in the tunica media than that from Dnmt1^{WT} (Fig. 5E). Parallelly, an enhanced macrophage (CD68$^+$) accumulation was observed in the tunica media of the Dnmt1^{sKO} mice (Fig. S13). In the functional assays, vasoconstriction of thoracic aorta evoked by KCl or by phenylephrine
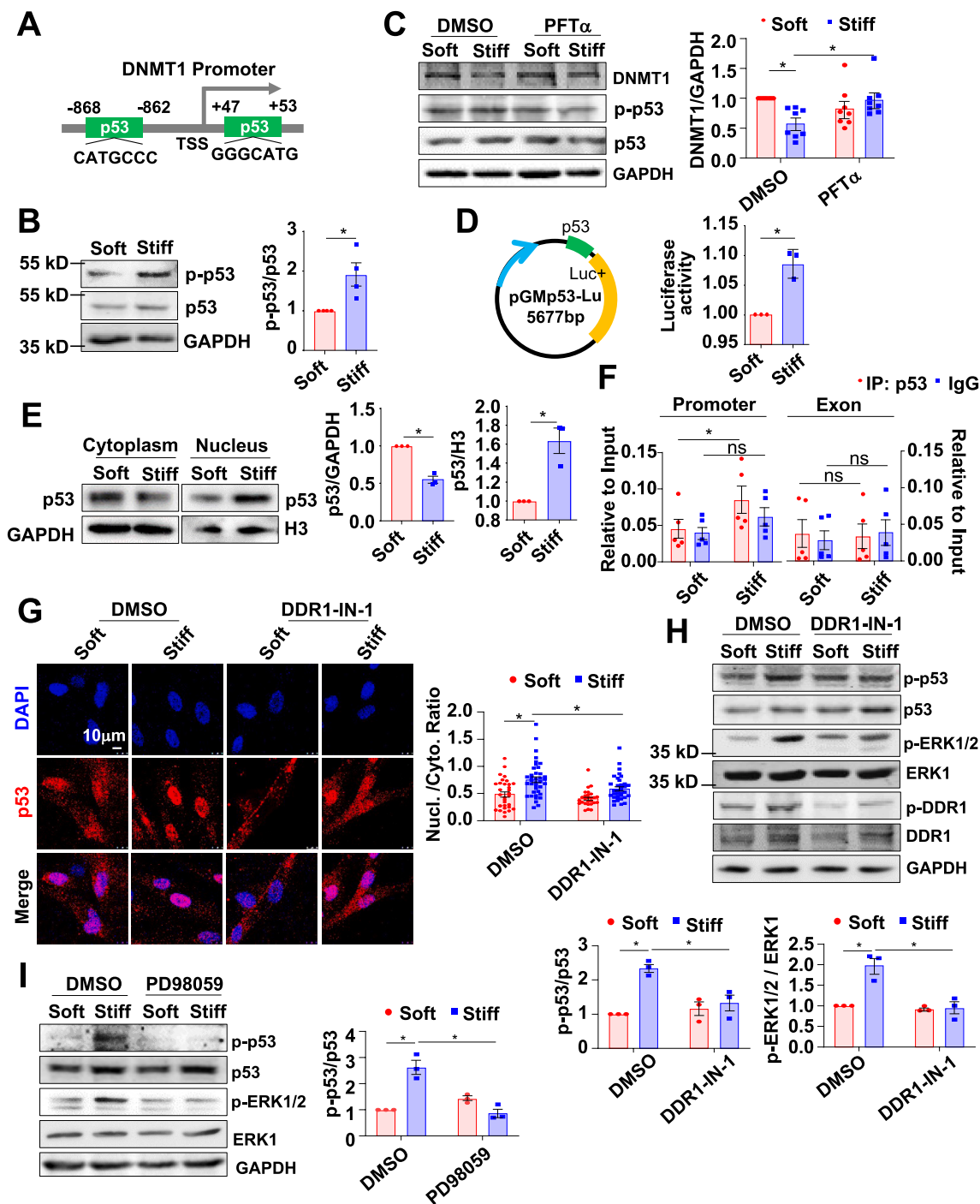
Fig. 4. The ERK-p53 pathway is involved in the DDR1-mediated DNMT1 regulation by matrix stiffness. *(A)* Schematic diagram of the promoter regions of human DNMT1 gene. Two p53 binding sites (−868~-862 and + 47~+53) are indicated. *(B)* Representative Western blots (left panel) and their quantification (right panel) indicating the phosphorylated p53 at Ser15 (p-p53) and total p53 levels in SMCs grown on gels. *(C)* Representative Western blots indicating the DNMT1, p-p53 and p53 levels in SMCs grown on gels. The cells were pre-treated with PFT-α (a reagent inhibiting p53 activity) or DMSO. *(D)* Luciferase assay to determine p53 activity in SMCs grown on gels. The schematic illustration of reporter plasmid construction is shown in the left panel. Each dot means one independent experiment. *(E)* Western blots (left panels) and their quantification (right panels) indicating the p53 accumulation in the nucleus and cytoplasm of SMCs cultured on gels. *(F)* Chromatin immunoprecipitation to determine the binding of p53 to the promoter regions of DNMT1 in SMCs grown on gel substrates. Left panel: a DNMT1 promoter region. Right panel: a DNMT1 exon region. Each dot means one independent experiment. *(G)* Immunofluorescent staining of p53 in SMCs grown on gel substrates. The cells were pre-treated for 3 h with DDR1-IN-1 or DMSO. Quantification of the ratio of nuclear p53 signal versus the cytoplasmic p53 is shown in the lower panel. Each dot represents one cell. *(H)* and *(I)* Western blots and their quantification indicating the levels of the indicated proteins in SMCs grown on gels. The cells were pretreated with DDR1 inhibitor DDR1-IN-1, ERK inhibitor PD98059, or DMSO. For Western blotting assay, shown are representative blots from at least 3 independent experiments. Semi-quantification of indicated proteins were performed by using the ImageJ software. *P < 0.05 vs. the indicated group.
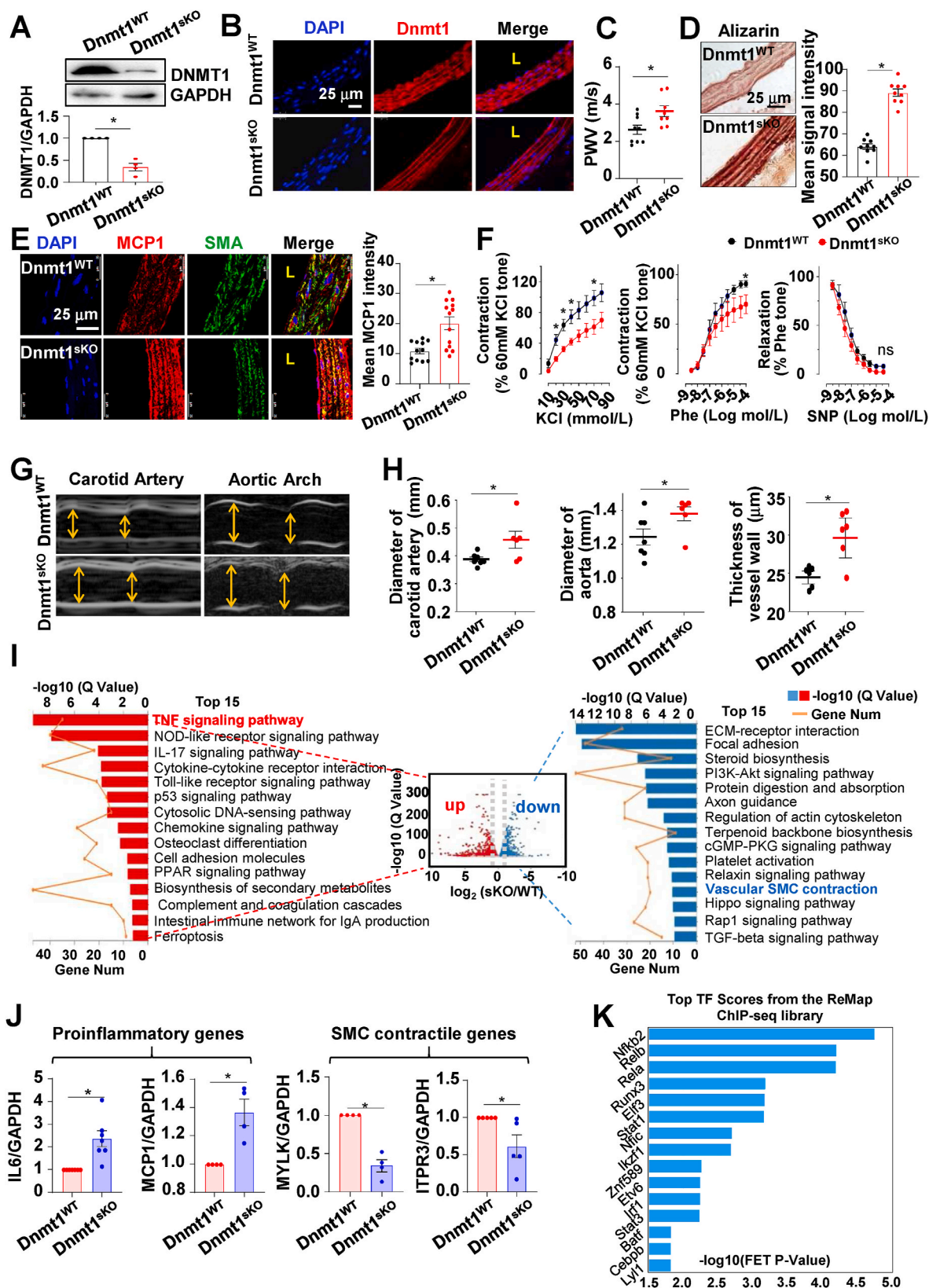
(caption on next page)

Fig. 5. Depletion of Dnmt1 in vSMC leads to vascular dysregulation and changes in gene expression. *(A)* Western blotting assay to determine the expression of DNMT1 in the aortas of Dnmt1[WT] and Dnmt1[sKO] mice. Shown are representative blots from at least 3 independent experiments. Semi-quantification of the blots was shown in the lower panel. *(B)* Representative images of DNMT1 immunofluorescence in aortas from DNMT[WT] and DNMT1[sKO] mice. *(C)* Pulse wave velocity (PWV) in the carotid arteries in Dnmt1[WT] and Dnmt1[sKO] mice. One dot represents one mouse. *(D)* Representative Alizarin red S staining and its quantification in aortas from DNMT[WT] and DNMT1[sKO] mice. *(E)* Representative images and the quantification of MCP1 and SMC marker SMA immunofluorescence in aortas from DNMT[WT] and DNMT1[sKO] mice. *(F)* Vasocontraction evoked by KCl or phenylephrine (Phe), and vasorelaxation in response to nitroprusside (SNP) in the thoracic aortas from DNMT[WT] and DNMT1[sKO] mice. n = 4 mice in each group. *(G)* Representative ultrasound images in the carotid artery and aortic arch Dnmt1[WT] and Dnmt1[sKO] mice. *(H)* Diameter and wall thickness of the carotid artery and aortic arch in Dnmt1[WT] and Dnmt1[sKO] mice were calculating from the ultrasound measurements. Each dot means one mouse. *$P < 0.05$ vs the indicated group. *(I)* Volcano-plot and KEGG pathway analysis of the differentially expressed genes (DEGs) in the aortas of Dnmt1[sKO] vs. Dnmt1[WT]mice. The top 15 KEGG terms for genes up-regulated by Dnmt1 depletion are shown in red, while those down regulated are shown in blue. *(J)* Quantitative RT-PCR to measure the expressions of IL6, MCP1, MYLK and ITPR3 in the Dnmt1-deficient or WT mouse SMCs (n = 4–7). *(K)* DEGs in *(I)* were subjected to the transcription factor enrichment analysis, the top 15 enriched transcription factors were presented. L: lumen. *$P < 0.05$ vs. the indicated group. (For interpretation of the references to color in this figure legend, the reader is referred to the Web version of this article.)

(Phe) was found to be markedly decreased with Dnmt1 depletion, while there was no significant difference in vasodilatation in response to sodium nitroprusside (SNP) between Dnmt1[sKO] and Dnmt1[WT] (Fig. 5F). In addition, ultrasound imaging revealed that the diameters of both carotid artery and aortic arch were increased in Dnmt1[sKO] mice, and that the thickness of carotid arterial wall increased as well (Fig. 5G and H). Collectively, these results demonstrate that Dnmt1 depletion in vSMCs results in arterial stiffening and vascular dysfunction in terms of inflammation, aortic dilation and loss of contractility.

3.6. Depletion of Dnmt1 causes changes in gene expression in vascular wall

To explore the mechanisms by which SMC Dnmt1 deficiency causes vascular dysfunction, we collected RNAs from the aortas (endothelium and adventitia removed) of Dnmt1[WT] and Dnmt1[sKO] mice to perform transcriptional profiling. The data were analyzed (the quality control metrics were shown in Figs. S14) and a volcano plot was constructed to visualize the DEGs between the two groups. The Q-value (adjusted *P*-value) threshold was set to 0.05, and |log₂ fold change| threshold to 0.5. The plot shows that 1324 genes were up regulated, whereas 1166 genes were down regulated in Dnmt1[sKO] mice, compared with that in Dnmt1[WT] (Fig. S15). KEGG pathways enrichment analysis of the up- and downregulated DEGs was performed and the top 15 pathways are presented (Fig. 5I). The upregulated DEGs were enriched in TNF signaling pathway, chemokine signaling pathway, p53 signaling pathway etc. The downregulated DEGs were enriched in pathways such as ECM-receptor interaction, focal adhesion, and vascular smooth muscle contraction (Fig. 5I). Given that the Dnmt1[sKO] vessels displayed proinflammatory and loss-of-contractility phenotypes (Fig. 5E and F), we focused on the TNF signaling and vascular smooth muscle contraction pathways, where the expressions of the DEGs are indicated in the heat map (Fig. S16A). GSEA indicated that the genes enriched in the TNF signaling pathway were up-regulated and the genes in controlling SMC contraction were down-regulated in Dnmt1[sKO] (Fig. S16B). The expressions of various DEGs was verified by quantitative RT-PCR (Fig. 5J). We further studied the transcription factors that might contribute to regulation of these DEGs based on the ChEA3 online tool (https://maayanlab.cloud/chea3/). 55 genes in these two pathways were subjected to the transcription factor enrichment analysis, and the top 15 enriched transcription factors were presented (Fig. 5K), suggestive of a multifunctional role of DNMT1 in vSMCs. Collectively, Dnmt1 deficiency causes dysregulation of proinflammatory and smooth muscle contractile genes and might consequently result in vascular dysfunction.

3.7. DDR1 inhibition alleviates arterial inflammation and stiffening

To study the role of DDR1 in arterial stiffening in vivo, we first utilized a CaCl₂-induced arterial calcification/stiffening mouse model. C57/BL6 wildtype mice aged 12 weeks were intraperitoneally injected daily with 0.2 mg/kg DDR1-IN-1 in saline or with the control solvent (DMSO in saline) for 5 days, subjected to local incubation of their

abdominal aortas with 0.5 mol/L CaCl₂ for 10 min on the 6th day, and the aortas were then harvested one week-post surgery for assays (Fig. 6A). Local incubation with CaCl₂ induced an increase in p-DDR1, which was suppressed upon treatment with DDR–IN–1 (Fig. 6B). Accordingly, DNMT1 repression caused by CaCl₂ incubation was eliminated by treatment with DDR–IN–1 (Fig. 6C), suggesting that DDR1 regulates DNMT1 expression. Furthermore, immunofluorescence detected increased MCP1 whereas decreased contractile marker SMMHC (Smooth muscle myosin heavy chain) staining in tunica media of the vessels with CaCl₂ incubation in the DMSO groups, indicative of SMC inflammation and loss of contractility, and that the changes could be diminished by DDR1-IN-1 (Fig. 6D). Consistently, infiltration of CD68^{+} macrophage into the tunica media was observed in the CaCl₂-treated vessels in the DMSO groups, but rarely seen in the DDR1-IN-1 groups (Fig. 6E), indicating that DDR1 inhibition counteracts the acute-injury-induced arterial inflammation. Phosphorylation of ERK1/2 and p53, arterial stiffening and calcium deposition in the vessels were successfully induced by incubation with CaCl₂; the induction could be eliminated by DDR1-IN-1 delivery (Figs. 6F, G, S17 and S18). These in vivo findings demonstrate that ECM stiffness promotes the phenotype of vSMC switch towards a proinflammatory state and aggravates arterial stiffening by activating DDR1.

We further utilized a chronic vascular stiffening model to study the role of DDR1-DNMT1 in a long-term. In this experiment, C57/BL6 mice aged 12 weeks were fed on a high adenine diet (0.2% adenine) for 6 weeks to induce vascular stiffening. During the diet, mice were intraperitoneally injected every 3 days with 0.2 mg/kg DDR1-IN-1 in saline or/and 0.2 mg/kg 5-Aza in saline. After 6-weeks feeding, PWV measurements were performed and then the aortas were harvested for assays (Fig. 7A). High adenine feeding induced an increase in p-DDR1 level, which could be suppressed by DDR1-IN-1 treatment (Fig. 7B). DNMT1 expression was decreased by adenine-feeding and the decrease was abolished with application of DDR1-IN-1 (Fig. 7C). As expected, DNMT1 expression was markedly inhibited by administration of 5-Aza (Fig. 7C). Adenine diet induced MCP1 accumulation, increase in stiffness, decrease in expression of SMC contractile marker SMMHC, and calcium deposition in the vessel wall; the effects were suppressed by sole administration of DDR1-IN-1 and de-suppressed by a combined treatment of DDR1-IN-1 and 5-Aza (Fig. 7D–G and S19), indicative of a role of the DDR1-DNMT1 axis in modulating vascular pathology. We also employed the Dnmt1[sKO] mice to verify the role of DNMT1 in arterial stiffening (Fig. S20A). Compared with Dnmt1[WT], the Dnmt1[sKO] mice were hypersusceptible to adenine diet, as evidenced by the increases in calcium deposition, MCP1 production, and PWV (Figs. S20B–F). Collectively, these results verified the role of DDR1-DNMT1 pathway in regulating arterial inflammation and stiffness.

3.8. The DDR1-DNMT1 signaling regulates ECM homeostasis and inflammation

To provide insight into the cellular mechanisms bridging vascular stiffness to vSMC inflammation, we measured the elastic moduli of
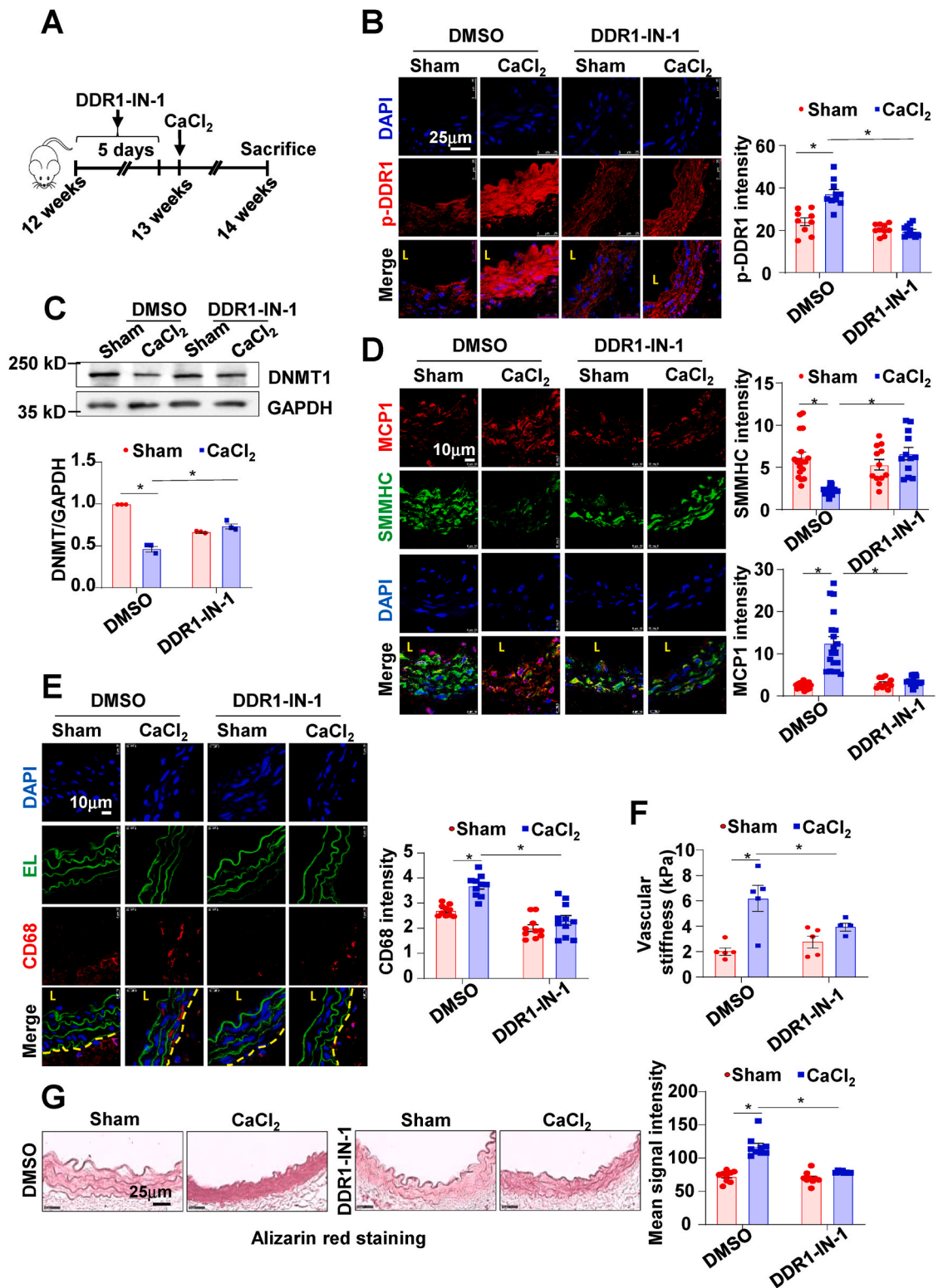
Fig. 6. DDR1 inhibition alleviates the acute vascular injury-induced arterial inflammation and stiffening. *(A)* Schematic diagram of the acute vascular injury model in mouse. The mice were subjected to repetitive intraperitoneal injections with DDR–IN–1 or DMSO. *(B)* Representative immunofluorescent staining and the quantification of p-DDR1 in the abdominal aorta from the $CaCl_2$-incubated or sham-operated mice. *(C)* Representative Western blots and the quantification of DNMT1 in arterial segments from the $CaCl_2$-incubated or sham-operated mice. *(D)* Representative immunofluorescent staining and the quantification of MCP1 and SMMHC in mouse aortas with or without $CaCl_2$-incubation. The mice were subjected to applications with DDR1-IN-1 or DMSO. *(E)* Representative immunofluorescent staining and the quantification of CD68 in mouse aortas with or without $CaCl_2$-incubation. The mice were subjected to applications with DDR1-IN-1 or DMSO. The border between the adventitia and the media is denoted by a dashed line. *(F)* The elastic moduli of the operated vessels in the indicated mice were measured by nanoindentation. Each dot represents one mouse. *(G)* Representative Alizarin red S staining and its quantification in the indicated aortas. Shown are representative images from at least 3 mice in each group. L: lumen. *$P < 0.05$ vs. the indicated group. (For interpretation of the references to color in this figure legend, the reader is referred to the Web version of this article.)
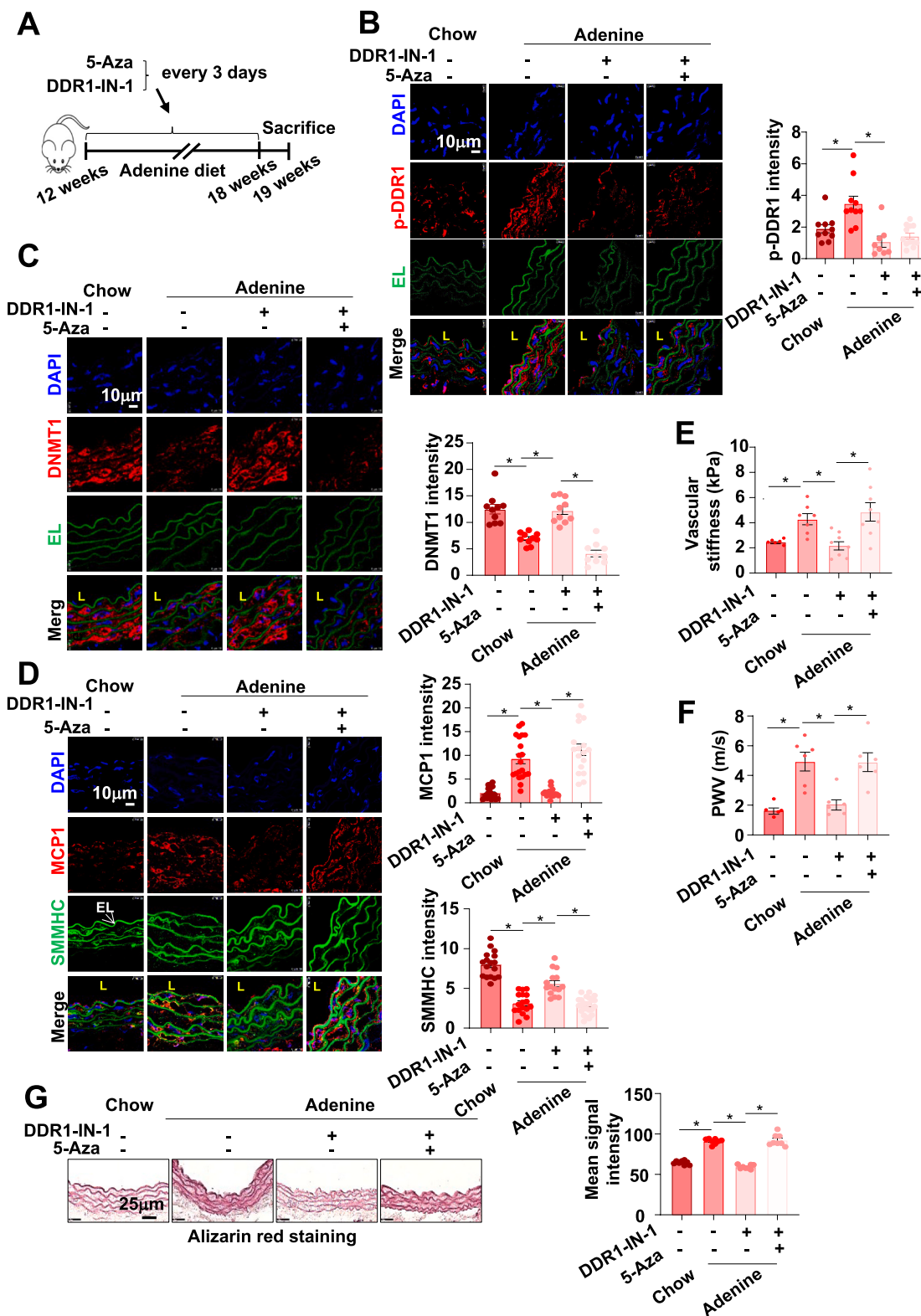
Fig. 7. DDR1-DNMT1 signaling regulates the adenine diet-induced arterial inflammation and stiffening. *(A)* Schematic diagram of the adenine diet-induced arterial stiffening model in mouse. The mice were subjected to repetitive intraperitoneal injections with DDR–IN–1 and/or 5-Aza or DMSO. *(B)* to *(D)* Representative immunofluorescent staining and the quantification of p-DDR1 *(B)*, DNMT1 *(C)*, MCP1 and SMMHC *(D)* in the abdominal aorta from mice with the indicated treatments. *(E)* The elastic moduli of the aortas in the indicated mice were measured by nanoindentation. Each dot represents one mouse. *(F)* Pulse wave velocity (PWV) in the carotid arteries of mice with the indicated treatments. One dot represents a mouse. *(G)* Representative Alizarin red S staining and its quantification in aortas from the indicated treatments. Shown are representative images from at least 3 mice in each group. EL: elastic lamina, L: lumen. $*P < 0.05$ vs the indicated group. (For interpretation of the references to color in this figure legend, the reader is referred to the Web version of this article.)

single cells and the very adjacent ECM using nanoindentation (Fig. 8A, S21-24). The cellular stiffness of vSMCs on stiff substrates was much higher than that on soft (3.25 ± 0.29 kPa vs. 1.38 ± 0.24 kPa), demonstrating that the substrate stiffness determines cellular stiffness (Fig. 8B). Treatment of cells with DDR1-IN-1 resulted in a dramatic reduction of elastic modulus in vSMCs on stiff substrates to 1.19 ± 0.16 kPa (Fig. 8B). These data are in line with our prior work indicating that overexpression of DNMT1 could suppress the substrate stiffness-induced cellular stiffening and reverse the switch of cell phenotype from contractile to osteoblastic [2]. Treating the cells with DDR1-IN-1 reduced the stiffness of the cell-adjacent-ECM to a lower extent than that on stiff substrates with DMSO (Fig. 8C), suggestive of a contribution of DDR1 to ECM remodeling by the ECM-surrounded cells. Interestingly, we found that the ECM stiffness could also be increased by ad-shDNMT1-mediated DNMT1 silencing while reduced by DNMT1 overexpression (Fig. 8D and E). Collectively, these observations indicated that DDR1 and DNMT1 regulate the cellular responses to matrix stiffness and ECM homeostasis. We then sought to answer the question as to whether the DDR1-DNMT1 pathway mediates the stiffness-induced vSMC inflammation. VSMC pretreated with DMSO, DDR1-IN1-1, 5-Aza, or the combination of DDR1-IN1-1 and 5-Aza were grown on gel substrates, and the expressions of proinflammatory MCP1and IL6 in vSMCs, migration of macrophages towards the vSMCs grown on gels, as well as the ECM stiffness in the vSMC-adjacent areas were measured. We observed dramatic increases in MCP1/IL6 expressions, macrophage attraction, and ECM stiffening in cells on stiff vs. soft gels with DMSO treatment, and that the increases were attenuated by DDR1-IN-1 and were re-activated by a combination of DDR1-IN-1 and 5-Aza (Fig. 8F–I and S25). Altogether, the findings demonstrate that DDR1-DNMT1 pathway mediates the substrate stiffness-elicited functional outcomes including ECM remodeling and proinflammatory responses.

4. Discussion

Although insufficient DNMT1 expression and DNA hypomethylation have been implicated in vSMC pathophysiology [47], our understanding about how the expression of DNMT1 is mechanically regulated remains rudimentary. Here, we demonstrate a mechanism that ECM stiffness activates DDR1 in a collagen-independent way to cause ERK1/2 phosphorylation, which leads to activation of p53 to suppress the transcription of DNMT1, resulting in matrix remodeling, wall inflammation, and consequent severe arterial stiffening. In clinical specimens of atherosclerotic plaques from patients with carotid occlusive diseases, increased DDR1 phosphorylation was found. Pharmacological inhibition of DDR1 attenuates vascular stiffening and inflammation and the alleviatory effects of DDR1 inhibition could be eliminated by DNMT1 inhibition. These findings suggest a previously uncharacterized role of vSMC DDR1 in perceiving the mechanical microenvironments and down-regulating expression of DNMT1, while DNMT1 impairment is linked to vascular pathologies. Furthermore, our results demonstrate that vSMCs and ECM interact in a positive feedback loop to drive arterial remodeling, which alters the mechanical properties of the tissue.

The impacts of ECM mechanics on the behavior and cell fate of vSMC have been studied by use of synthetic hydrogels as culture substrates [2, 48–50]. By using hydrogel substrates possessing defined elastic moduli, our previous study has demonstrated a critical modulator DNMT1 that responds to the ECM stiffness and negatively regulates arterial stiffening via maintaining the contractile phenotype of vSMCs [2]. A recent study by Tian et al. also indicates an involvement of TNF-β signaling pathway in mediating the matrix stiffness-regulated phenotypic switch of vSMC [51]. However, these studies did not explain how matrix stiffness is perceived by and subsequently transduced to biochemical signals in vSMCs. We initiated the present study from searching for mechanosensors or mechanosensitive proteins with an inhibitor-based screening. We found that inhibition of an RTK DDR1 could abolish the substrate stiffening-provoked repression on DNMT1 expression. DDR1 has been recently extensively studied in various tumor cells, epithelial cells, and fibroblasts as a contributor to tumor cancer metastasis and tissue fibrosis [22,23]. The first study uncovers the mechanosensitive function of DDR1 was reported by Ghosh and the colleagues [25]. Their work indicated a mechanotransduction pathway by DDR1-JNK1-JunB to modulate the ECM stiffness-stimulated growth of breast cancer cells. Bendeck et al. extended the research to vSMC and discovered that DDR1 cooperates with Rho A to sense ECM stiffness in a collagen-dependent manner to promote vSMC calcification [26]. In the present study, using comprehensive approaches including AFM, super-resolution microscopy, and peptide blocking, we demonstrated that DDR1 is indeed activated by matrix stiffness and the functional outcomes are mediated by the DDR1-DNMT1 axis. A major finding of our study is that the matrix stiffness-induced DDR1 activation can be independent of its ligand, collagen. In prior studies, mechanotransduction through DDR1 requires the DDR1-mediated cell adhesion to collagen [24,26,52], as those studies have shown that ligand binding is essential for DDR1 activation. In comparison, our study revealed that substrate stiffness solely could activate DDR1 phosphorylation, receptor oligomerization/clustering, and the receptor-ligand interaction in cells on fibronectin-coated PA gels, indicative of a collagen-independent activation of DDR1. To the best of our knowledge this is the first study reporting the independency. In search of the downstream effector molecules, we found that inhibition of DDR1 in cells on collagen- or fibronectin-coated gel substrates de-suppressed the matrix stiffness-downregulated DNMT1 expression. These results are in agreement with our previous findings that growing the cells on stiff substrate resulted in DNMT1 down-regulation no matter that the gels were coated with fibronectin, collagen type I, or laminin [2]. While it is possible that activation of DDR1 is secondary to the activation of other known mechanosensitive proteins such as $\alpha_5\beta_1$-integrin [53] and caveolin-1 [54], DDR1 may also direct the mechanoperception role of other mechanosensitive proteins, as studies have indicated that DDR1 regulates β1 integrin bindings with collagen and promotes the α1β1 and α2β1 integrin-mediated cell adhesion [55, 56], suggesting functional redundancy of DDR1 and integrins in regulating cell-matrix interactions. Nevertheless, there is a possibility that the collagen-independent mechanical activation of DDR1 may require the primary activation of other mechanosensors.

Transcriptional regulation of DNMT1 consists of various pathways, e. g., the RAS-AP-1, PI3/PKB, Rb/E2F and p53/Sp1 pathways [57]. P53 can regulate DNMT1 expression by forming a complex with specificity protein 1 (Sp1) protein to inhibit the Sp1-dependent DNMT1 transcription [58,59]. Although previous study in breast cancer cells has reported that ECM stiffness induces p53 activation and nuclear accumulation [60], the stiffness-activation of p53 has not been documented in vSMCs prior to the present study. Here, we observed that p53 was activated in vSMCs on the stiff matrix, as is evident from p53 phosphorylation and nuclear translocation. Our data revealed a role of p53 in response to matrix stiffness to modulate DNMT1 expression by showing that decreasing p53 activity in cells on stiff substrates could de-suppress the stiffness-inhibited DNMT1 expression. An important information that inspired us to connect the mechanical activation of p53 with DDR1 is provided by early report indicating that the irradiation-activated DDR1 positively regulates phosphorylation and nuclear accumulation of p53 [61]. We tested the potential connections in our in vitro model and found that the substrate stiffness-induced p53 phosphorylation could be blocked by DDR1 inhibition. The link between matrix stiffness and ERK activation has been implicated in mesenchymal stem cells and endothelial cells [62–64], and there has been report on the collagen type I-stimulated DDR1 activation to promote ERK phosphorylation in vSMCs [45]. We tested the involvement of ERK1/2 in the mechanotransduction pathway downstream of DDR1 and our findings indicated that ERK1/2 phosphorylation increases with matrix stiffness in vSMCs, while this response was attenuated in DDR1-inhibited cells, suggesting that DDR1 is required for the stiffness-elicited ERK activation. Altogether, our studies support a mechanism that the DDR1-ERK-p53 signaling mediates
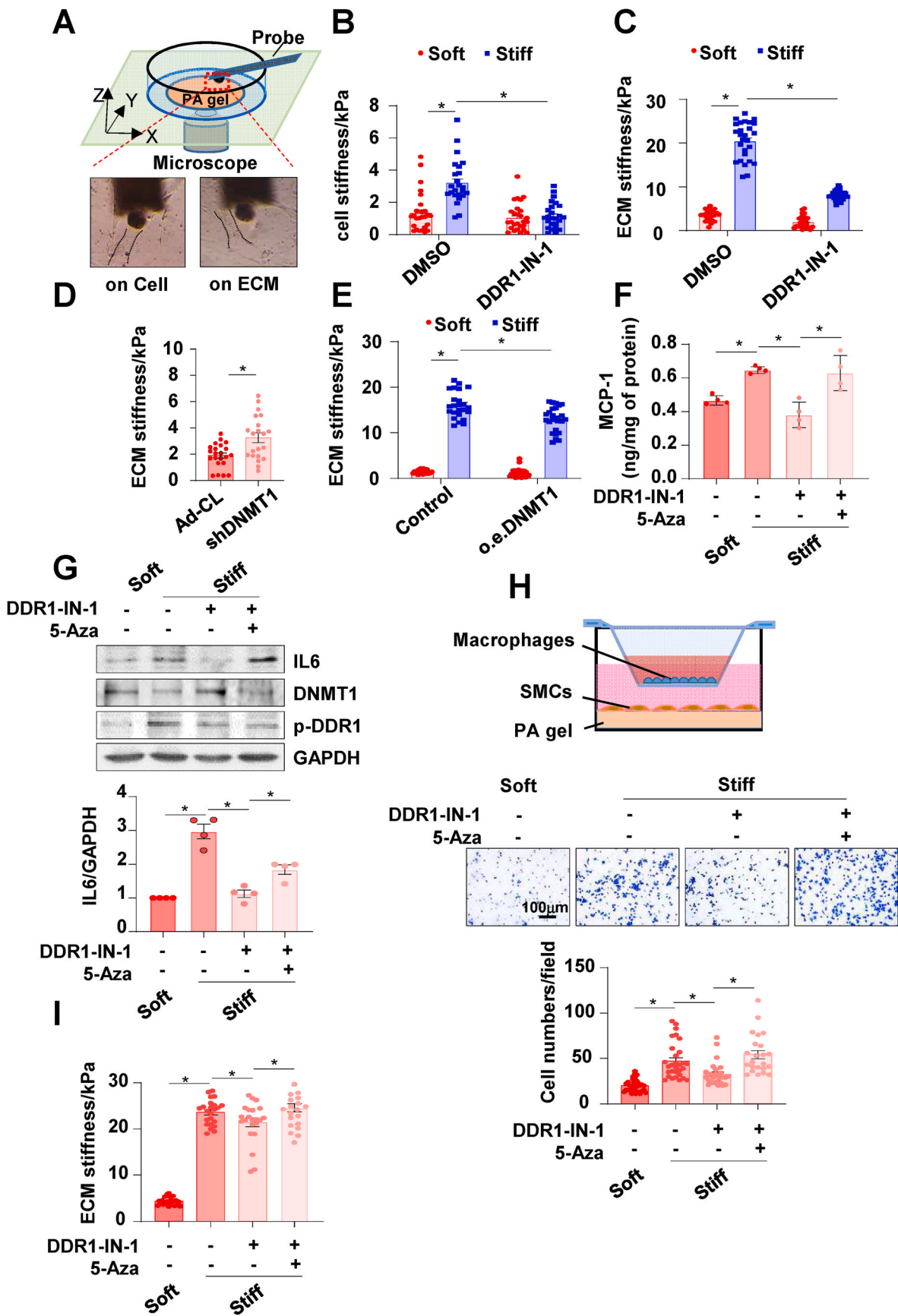
(caption on next page)

Fig. 8. The DDR1-DNMT1 pathway regulates ECM stiffness and vSMC inflammation. (A) Schematic diagram illustrating measurement methods for testing the elastic moduli of an on-gel cultured single cell and the cell-adjacent extracellular matrix (ECM) by nanoindentation. **(B)** to **(E)** The elastic moduli of on-gel cultured SMCs and the cell-adjacent ECM measured by nanoindentation. Some cells were pre-treated with DDR1-IN-1 or DMSO **(B and C)**, some cells were infected with adenovirus expressing shDNMT1 or the control adenovirus expressing GFP (Ad-CL) **(D)**, and others were transfected with plasmids expressing the human DNMT1 gene (o.e. DNMT1) or the control empty vector **(E)**. In **(B)**, each dot represents one cell, and in **(C)** to **(E)**, each dot represents one point on matrix adjacent to the cell body. 20 to 30 measurements were taken in each experiment. From **(F)** to **(I)**, SMCs were pre-treated with DMSO, DDR1-IN1-1, or the combination of DDR1-IN1-1 and 5-Aza and were cultured on gel substrates. **(F)** and **(G)** The protein levels of MCP1 and IL6 were measured by ELISA or Western blot in SMCs with the indicated treatments. **(H)** Transwell migration assay in RAW 264.7 macrophages that were co-cultured with SMCs grown on gels. The SMCs were subjected to the indicated treatments. The migrated macrophages were stained with crystal violet and cell numbers were counted. For quantification, each dot represents one field under the microscope. **(I)** The elastic moduli of the SMC-adjacent ECM were measured. The cells were subjected to the indicated treatments. *$P < 0.05$ vs the indicated group. (For interpretation of the references to color in this figure legend, the reader is referred to the Web version of this article.)

the matrix stiffness-regulated DNMT1 transcription and hint at breaking the signaling cascade as a potential therapeutic target for treating the stiffness-induced vSMC dysfunction.

The functional roles of DDR1-DNMT1 axis in vSMC have not been fully understood. Early study has shown that systemic deficiency of DDR1 attenuates atherosclerotic calcification [65]. Consistently, our prior study indicated that inhibition of DNMT1 by intraperitoneal injection with a DNMT1 inhibitor facilitates arterial stiffening and calcification, hinting at functional interactions that link DNMT1 to ECM remodeling [2]. However, pharmacological inhibitors used to interrogate DNMT1 function were non-specific either for the target gene or for vSMC, thus highlighting the need for tissue-specific depletion of DNMT1. By using Dnmt1^{sKO} and Dnmt1^{WT} mice, the present study demonstrated a positive contribution of vSMC Dnmt1 to vascular contractility and a negative correlation between Dnmt1 and wall inflammation/stiffness. Transition of vSMC phenotype from contractile to proinflammatory caused by Dnmt1-deficiency can attract monocyte/macrophage infiltration, prime an osteogenic phenotype of vSMCs themselves, and in turn exacerbate ECM stiffness. In agreement with these functional findings, we also discovered upregulation of proinflammatory genes and downregulation of contractile genes in vSMCs from Dnmt1^{sKO} mice. In addition, our study identified the DDR1-DNMT1 pathway as an important player in regulating vascular inflammation and matrix homeostasis by employing loss-of-function approaches in the acute injury and chronic kidney failure-induced arterial stiffening models. In review of the fact that vSMCs synthesize ECM proteins and can produce proinflammatory molecules to contribute to tissue remodeling, our study illustrated a feedforward regulation of DDR1-DNMT1 pathway in vSMCs over ECM stiffness by presenting evidence that manipulating either DDR1 or DNMT1 in vSMCs could change the mechanical properties of the cell-adjacent ECM and modulate arterial stiffness.

As DDR1 activation can be blocked by pharmacological inhibitors and DNA methylation is known to be reversible, the DDR1-DNMT1 axis might be regarded as a promising target for therapeutic interventions. In this respect, our findings offer insight into mechanotherapeutic strategies aimed at ameliorating the mechanical microenvironments of the vessel wall to improve the vSMC and vascular functions. Furthermore, mechanobiological study in vasculature may shed lights on the design and development of new tissue-engineered vascular scaffolds for achieving appropriate scaffolding mechanics and bioactivity. Indeed, prior attempts have been made to reach some of these objectives including the development of scaffolding materials with ideal mechanical properties and bioacitivities providing mechanical cues to guide cell behaviors during vascular regeneration [66,67]. Thus, we believe that the potential future applications of our study are numerous and promising.

CRediT authorship contribution statement

Jin Wang: Conceptualization, Writing, Data curation, Visualization, Methodology, Formal analysis. **Si-an Xie:** Methodology, Formal analysis, Data curation. **Ning Li:** Methodology, Software. **Tao Zhang:** Resources. **Weijuan Yao:** Conceptualization. **Hucheng Zhao:**

Conceptualization. **Wei Pang:** Conceptualization. **Lili Han:** Project administration. **Jiayu Liu:** Validation. **Jing Zhou:** Supervision, Funding acquisition, Conceptualization, Writing, Project administration.

Declaration of competing interest

The authors report no commercial or proprietary interest in any product or concept discussed in this article.

Appendix A. Supplementary data

Supplementary data to this article can be found online at https://doi.org/10.1016/j.bioactmat.2022.01.012.

References

[1] D.A. Chistiakov, A.N. Orekhov, Y.V. Bobryshev, Vascular smooth muscle cell in atherosclerosis, Acta Physiol. 214 (1) (2015) 33–50.

[2] S.-A. Xie, T. Zhang, J. Wang, F. Zhao, Y.-P. Zhang, W.-J. Yao, S.S. Hur, Y.-T. Yeh, W. Pang, L.-S. Zheng, Y.-B. Fan, W. Kong, X. Wang, J.-J. Chiu, J. Zhou, Matrix stiffness determines the phenotype of vascular smooth muscle cell in vitro and in vivo: role of DNA methyltransferase 1, Biomaterials 155 (2018) 203–216.

[3] J.P. Stegemann, H. Hong, R.M. Nerem, Mechanical, biochemical, and extracellular matrix effects on vascular smooth muscle cell phenotype, J. Appl. Physiol. 98 (6) (2005) 2321–2327.

[4] J.P. Stegemann, R.M. Nerem, Phenotype modulation in vascular tissue engineering using biochemical and mechanical stimulation, Ann. Biomed. Eng. 31 (4) (2003) 391–402.

[5] A. Rezvani-Sharif, M. Tafazzoli-Shadpour, A. Avolio, Progressive changes of elastic moduli of arterial wall and atherosclerotic plaque components during plaque development in human coronary arteries, Med. Biol. Eng. Comput. 57 (3) (2019) 731–740.

[6] A.W. Orr, N.E. Hastings, B.R. Blackman, B.R. Wamhoff, Complex regulation and function of the inflammatory smooth muscle cell phenotype in atherosclerosis, J. Vasc. Res. 47 (2) (2010) 168–180.

[7] V. Sorokin, K. Vickneson, T. Kofidis, C.C. Woo, X.Y. Lin, R. Foo, C.M. Shanahan, Role of vascular smooth muscle cell plasticity and interactions in vessel wall inflammation, Front. Immunol. 11 (2020) 599415.

[8] M. Orejudo, A.B. García-Redondo, R.R. Rodrigues-Diez, R. Rodrigues-Díez, L. Santos-Sanchez, A. Tejera-Muñoz, J. Egido, R. Selgas, M. Salaices, A.M. Briones, M. Ruiz-Ortega, Interleukin-17A induces vascular remodeling of small arteries and blood pressure elevation, Clin. Sci. 134 (5) (1979) 513–527, 2020.

[9] I. Mozos, C. Malainer, J. Horbańczuk, C. Gug, D. Stoian, C.T. Luca, A.G. Atanasov, Inflammatory markers for arterial stiffness in cardiovascular diseases, Front. Immunol. 8 (2017) 1058.

[10] S. Park, E.G. Lakatta, Role of inflammation in the pathogenesis of arterial stiffness, Yonsei Med. J. 53 (2) (2012) 258–261.

[11] A. Portela, M. Esteller, Epigenetic modifications and human disease, Nat. Biotechnol. 28 (10) (2010) 1057–1068.

[12] A. Greißel, M. Culmes, R. Napieralski, E. Wagner, H. Gebhard, M. Schmitt, A. Zimmermann, H.-H. Eckstein, A. Zernecke, J. Pelisek, Alternation of histone and DNA methylation in human atherosclerotic carotid plaques, Thromb. Haemostasis 114 (8) (2015) 390–402.

[13] O. Hiltunen Mikko, S. Ylä-Herttuala, DNA methylation, smooth muscle cells, and atherogenesis, Arterioscler. Thromb. Vasc. Biol. 23 (10) (2003) 1750–1753.

[14] S.M. Yu, S.J. Kim, DNA-hypomethylating agent, 5'-azacytidine, induces cyclooxygenase-2 expression via the PI3-kinase/Akt and extracellular signal-regulated kinase-1/2 pathways in human HT1080 fibrosarcoma cells, Int. J. Oncol. 47 (4) (2015) 1469–1475.

[15] S. Lee, H.S. Kim, K.H. Roh, B.C. Lee, T.H. Shin, J.M. Yoo, Y.L. Kim, K.R. Yu, K. S. Kang, K.W. Seo, DNA methyltransferase inhibition accelerates the immunomodulation and migration of human mesenchymal stem cells, Sci. Rep. 5 (2015) 8020.

[16] M.S. Avendaño, S. Martínez-Revelles, A. Aguado, M.R. Simões, M. González-Amor, R. Palacios, P. Guillem-Llobat, D.V. Vassallo, L. Vila, J. García-Puig, L.M. Beltrán, M.J. Alonso, M.V. Cachofeiro, M. Salaices, A.M. Briones, Role of COX-2-derived PGE2 on vascular stiffness and function in hypertension, Br. J. Pharmacol. 173 (9) (2016) 1541–1555.

[17] A.M. Gorabi, P.E. Penson, M. Banach, M. Motallebnezhad, T. Jamialahmadi, A. Sahebkar, Epigenetic control of atherosclerosis via DNA methylation: a new therapeutic target? Life Sci. 253 (2020) 117682.

[18] H. Lv, L. Li, M. Sun, Y. Zhang, L. Chen, Y. Rong, Y. Li, Mechanism of regulation of stem cell differentiation by matrix stiffness, Stem Cell Res. Ther. 6 (1) (2015) 103.

[19] D. Ngai, M. Lino, M.P. Bendeck, Cell-matrix interactions and matricrine signaling in the pathogenesis of vascular calcification, Front. Cardiovasc. Med. 5 (2018) 174.

[20] J. Schlessinger, Direct binding and activation of receptor tyrosine kinases by collagen, Cell 91 (7) (1997) 869–872.

[21] H. Rammal, C. Saby, K. Magnien, L. Van-Gulick, R. Garnotel, E. Buache, H. El Btaouri, P. Jeannesson, H. Morjani, Corrigendum: discoidin domain receptors: potential actors and targets in cancer, Front. Pharmacol. 7 (2016) 346.

[22] B. Leitinger, Discoidin domain receptor functions in physiological and pathological conditions, Int. Rev. Cell Mol. Biol. 310 (2014) 39–87.

[23] N.M. Coelho, C.A. McCulloch, Mechanical signaling through the discoidin domain receptor 1 plays a central role in tissue fibrosis, Cell Adhes. Migrat. 12 (4) (2018) 348–362.

[24] N.M. Coelho, P.D. Arora, S. van Putten, S. Boo, P. Petrovic, A.X. Lin, B. Hinz, C. A. McCulloch, Discoidin domain receptor 1 mediates myosin-dependent collagen contraction, Cell Rep. 18 (7) (2017) 1774–1790.

[25] S. Ghosh, K. Ashcraft, M.J. Jahid, C. April, C.M. Ghajar, J. Ruan, H. Wang, M. Foster, D.C. Hughes, A.G. Ramirez, T. Huang, J.-B. Fan, Y. Hu, R. Li, Regulation of adipose oestrogen output by mechanical stress, Nat. Commun. 4 (2013) 1821.

[26] D. Ngai, M. Lino, K.E. Rothenberg, C.A. Simmons, S. Fernandez-Gonzalez, M. P. Bendeck, DDR1 (discoidin domain receptor-1)-RhoA (Ras Homolog family member A) Axis senses matrix stiffness to promote vascular calcification, Arterioscler. Thromb. Vasc. Biol. 40 (7) (2020) 1763–1776.

[27] H. Li, T. Rauch, Z.-X. Chen, P.E. Szabó, A.D. Riggs, G.P. Pfeifer, The histone methyltransferase SETDB1 and the DNA methyltransferase DNMT3A interact directly and localize to promoters silenced in cancer cells, J. Biol. Chem. 281 (28) (2006) 19489–19500.

[28] J.R. Tse, A.J. Engler, Preparation of hydrogel substrates with tunable mechanical properties, Curr.Protoc. Cell Biol. 47 (1) (2010), 10.6.1-.6.6.

[29] E.A. Klein, L. Yin, D. Kothapalli, P. Castagnino, F.J. Byfield, T. Xu, I. Levental, E. Hawthorne, P.A. Janmey, R.K. Assoian, Cell-cycle control by physiological matrix elasticity and in vivo tissue stiffening, Curr. Biol. 19 (18) (2009) 1511–1518.

[30] L.N. Hachehouche, N. Chetoui, F. Aoudjit, Implication of discoidin domain receptor 1 in T cell migration in three-dimensional collagen, Mol. Immunol. 47 (9) (2010) 1866–1869.

[31] G. Mattei, G. Gruca, N. Rijnveld, A. Ahluwalia, The nano-epsilon dot method for strain rate viscoelastic characterisation of soft biomaterials by spherical nano-indentation, J. Mech. Behav. Biomed. Mater. 50 (2015) 150–159.

[32] N. Li, H. Yang, M. Wang, S. Lü, Y. Zhang, M. Long, Ligand-specific binding forces of LFA-1 and Mac-1 in neutrophil adhesion and crawling, Mol. Biol. Cell 29 (4) (2018) 408–418.

[33] D. Deshpande, M. Grieshober, F. Wondany, F. Gerbl, R. Noschka, J. Michaelis, S. Stenger, Super-resolution microscopy reveals a direct interaction of intracellular Mycobacterium tuberculosis with the antimicrobial peptide LL-37, Int. J. Mol. Sci. 21 (18) (2020).

[34] H. Wang, Z. Xiao, J. Zheng, J. Wu, X.-L. Hu, X. Yang, Q. Shen, ZEB1 represses neural differentiation and cooperates with CTBP2 to dynamically regulate cell migration during neocortex development, Cell Rep. 27 (8) (2019) 2335–2353, e6.

[35] R.C. Lynn, E.W. Weber, E. Sotillo, D. Gennert, P. Xu, Z. Good, H. Anbunathan, J. Lattin, R. Jones, V. Tieu, S. Nagaraja, J. Granja, C.F.A. de Bourcy, R. Majzner, A. T. Satpathy, S.R. Quake, M. Monje, H.Y. Chang, C.L. Mackall, c-Jun overexpression in CAR T cells induces exhaustion resistance, Nature 576 (7786) (2019) 293–300.

[36] K. Lajtai, R. Tarszabó, B. Bányai, B. Péterffy, D. Gerszi, É. Ruisanchez, R.E. Sziva, Á. Korsós-Novák, R. Benkő, L. Hadjadj, Z. Benyó, E.M. Horváth, G. Masszi, S. Várbíró, Effect of vitamin D status on vascular function of the aorta in a rat model of PCOS, Oxid. Med. Cell. Longev. (2021) 8865979, 2021.

[37] C. Mihai, M. Chotani, T.S. Elton, G. Agarwal, Mapping of DDR1 distribution and oligomerization on the cell surface by FRET microscopy, J. Mol. Biol. 385 (2) (2009) 432–445.

[38] D.S. Corcoran, V. Juskaite, Y. Xu, F. Görlitz, Y. Alexandrov, C. Dunsby, P.M. W. French, B. Leitinger, DDR1 autophosphorylation is a result of aggregation into dense clusters, Sci. Rep. 9 (1) (2019) 17104.

[39] C. Mihai, M. Chotani, T.S. Elton, G. Agarwal, Mapping of DDR1 distribution and oligomerization on the cell surface by FRET microscopy, J. Mol. Biol. 385 (2) (2009), 0-445.

[40] M. Mani, U. Lee, N.A. Yoon, H. Kim, M. Ko, W. Seol, Y. Joe, H. Chung, B.J. Lee, C. Moon, W. Cho, J.W. Park, Developmentally regulated GTP-binding protein 2 coordinates Rab5 activity and transferrin recycling, Mol. Biol. Cell 27 (2015).

[41] D. Yeung, D. Chmielewski, C. Mihai, G. Agarwal, Oligomerization of DDR1 ECD affects receptor-ligand binding, J. Struct. Biol. 183 (3) (2013) 495–500.

[42] E. Faraci, M. Eck, B. Gerstmayer, A. Bosio, W.F. Vogel, An extracellular matrix-specific microarray allowed the identification of target genes downstream of discoidin domain receptors, Matrix Biol. 22 (4) (2003) 373–381.

[43] J. Loughery, M. Cox, L.M. Smith, D.W. Meek, Critical role for p53-serine 15 phosphorylation in stimulating transactivation at p53-responsive promoters, Nucleic Acids Res. 42 (12) (2014) 7666–7680.

[44] A.M. Bode, Z. Dong, Post-translational modification of p53 in tumorigenesis, Nat. Rev. Cancer 4 (10) (2004) 793–805.

[45] K.K. Lu, D. Trcka, M.P. Bendeck, Collagen stimulates discoidin domain receptor 1-mediated migration of smooth muscle cells through Src, Cardiovasc. Pathol. 20 (2) (2011) 71–76.

[46] M.-A. El Azreq, M. Kadiri, M. Boisvert, N. Pagé, P.A. Tessier, F. Aoudjit, Discoidin domain receptor 1 promotes Th17 cell migration by activating the RhoA/ROCK/MAPK/ERK signaling pathway, Oncotarget 7 (29) (2016) 44975–44990.

[47] B.G. Jorgensen, R.M. Berent, S.E. Ha, K. Horiguchi, K.C. Sasse, L.S. Becker, S. Ro, DNA methylation, through DNMT1, has an essential role in the development of gastrointestinal smooth muscle cells and disease, Cell Death Dis. 9 (5) (2018) 474.

[48] S.R. Peyton, C.B. Raub, V.P. Keschrumrus, A.J. Putnam, The use of poly(ethylene glycol) hydrogels to investigate the impact of ECM chemistry and mechanics on smooth muscle cells, Biomaterials 27 (28) (2006) 4881–4893.

[49] A. Shkumatov, M. Thompson, K.M. Choi, D. Sicard, K. Baek, D.H. Kim, D. J. Tschumperlin, Y.S. Prakash, H. Kong, Matrix stiffness-modulated proliferation and secretory function of the airway smooth muscle cells, Am. J. Physiol. Lung Cell Mol. Physiol. 308 (11) (2015) L1125–L1135.

[50] C.D. Hartman, B.C. Isenberg, S.G. Chua, J.Y. Wong, Vascular smooth muscle cell durotaxis depends on extracellular matrix composition, Proc. Natl. Acad. Sci. U. S. A. 113 (40) (2016) 11190–11195.

[51] B. Tian, X. Ding, Y. Song, W. Chen, J. Liang, L. Yang, Y. Fan, S. Li, Y. Zhou, Matrix stiffness regulates SMC functions via TGF-β signaling pathway, Biomaterials 221 (2019) 119407.

[52] C.M. Borza, Y. Su, T.-L. Tran, L. Yu, N. Steyns, K.J. Temple, M.J. Skwark, J. Meiler, C.W. Lindsley, B.R. Hicks, B. Leitinger, R. Zent, A. Pozzi, Discoidin domain receptor 1 kinase activity is required for regulating collagen IV synthesis, Matrix Biol. 57–58 (2017) 258–271.

[53] M. Riaz, M. Versaevel, D. Mohammed, K. Glinel, S. Gabriele, Persistence of fan-shaped keratocytes is a matrix-rigidity-dependent mechanism that requires α(5)β (1) integrin engagement, Sci. Rep. 6 (2016) 34141.

[54] R. Moreno-Vicente, D.M. Pavón, I. Martín-Padura, M. Catalá-Montoro, A. Díez-Sánchez, A. Quílez-Álvarez, J.A. López, M. Sánchez-Álvarez, J. Vázquez, R. Strippoli, M.A. Del Pozo, Caveolin-1 modulates mechanotransduction responses to substrate stiffness through actin-dependent control of YAP, Cell Rep. 25 (6) (2018) 1622–1635, e6.

[55] L.A. Staudinger, S.J. Spano, W. Lee, N. Coelho, D. Rajshankar, M.P. Bendeck, T. Moriarty, C.A. McCulloch, Interactions between the discoidin domain receptor 1 and β1 integrin regulate attachment to collagen, Biol. Open 2 (11) (2013) 1148–1159.

[56] H. Xu, D. Bihan, F. Chang, P.H. Huang, R.W. Farndale, B. Leitinger, Discoidin domain receptors promote α1β1- and α2β1-integrin mediated cell adhesion to collagen by enhancing integrin activation, PLoS One 7 (12) (2012) e52209-e.

[57] S. Kar, M. Deb, D. Sengupta, A. Shilpi, S. Parbin, J. Torrisani, S. Pradhan, S. Patra, An insight into the various regulatory mechanisms modulating human DNA methyltransferase 1 stability and function, Epigenetics 7 (9) (2012) 994–1007.

[58] R.-K. Lin, C.-Y. Wu, J.-W. Chang, L.-J. Juan, H.-S. Hsu, C.-Y. Chen, Y.-Y. Lu, Y.-A. Tang, Y.-C. Yang, P.-C. Yang, Y.-C. Wang, Dysregulation of p53/Sp1 control leads to DNA methyltransferase-1 overexpression in lung cancer, Cancer Res. 70 (14) (2010) 5807.

[59] S.R.M. Kinney, S. Pradhan, Chapter 9 - regulation of expression and activity of DNA (Cytosine-5) methyltransferases in mammalian cells, in: X. Cheng, R. M. Blumenthal (Eds.), Progress in Molecular Biology and Translational Science, vol. 101, Academic Press, 2011, pp. 311–333.

[60] T. Ebata, Y. Mitsui, W. Sugimoto, M. Maeda, K. Araki, H. Machiyama, I. Harada, Y. Sawada, H. Fujita, H. Hirata, K. Kawauchi, Substrate stiffness influences doxorubicin-induced p53 activation via ROCK2 expression, BioMed Res. Int. 2017 (2017) 5158961.

[61] P.P. Ongusaha, J-i Kim, L. Fang, T.W. Wong, G.D. Yancopoulos, S.A. Aaronson, S. W. Lee, p53 induction and activation of DDR1 kinase counteract p53-mediated apoptosis and influence p53 regulation through a positive feedback loop, EMBO J. 22 (6) (2003) 1289–1301.

[62] W. Wan, B. Cheng, C. Zhang, Y. Ma, A. Li, F. Xu, M. Lin, Synergistic effect of matrix stiffness and inflammatory factors on osteogenic differentiation of MSC, Biophys. J. 117 (1) (2019) 129–142.

[63] J.-H. Hwang, M.R. Byun, A.R. Kim, K.M. Kim, H.J. Cho, Y.H. Lee, J. Kim, M. G. Jeong, E.S. Hwang, J.-H. Hong, Extracellular matrix stiffness regulates osteogenic differentiation through MAPK activation, PLoS One 10 (8) (2015) e0135519–e.

[64] D.J. LaValley, M.R. Zanotelli, F. Bordeleau, W. Wang, S.C. Schwager, C. A. Reinhart-King, Matrix stiffness enhances VEGFR-2 internalization, signaling, and proliferation in endothelial cells, Converg. Sci. Phys. Oncol. 3 (2017), 044001.

[65] P.J. Ahmad, D. Trcka, S. Xue, C. Franco, M.Y. Speer, C.M. Giachelli, M.P. Bendeck, Discoidin domain receptor-1 deficiency attenuates atherosclerotic calcification and smooth muscle cell-mediated mineralization, Am. J. Pathol. 175 (6) (2009) 2686–2696.

[66] M. Iglesias-Echevarria, R. Johnson, M. Rafuse, Y. Ding, W. Tan, Vascular grafts with tailored stiffness and a ligand environment via multiarmed polymer sheath for expeditious regeneration, ACS Appl. Bio Mater. 4 (1) (2021) 545–558.

[67] X. Zhang, X. Chen, H. Hong, R. Hu, J. Liu, C. Liu, Decellularized extracellular matrix scaffolds: recent trends and emerging strategies in tissue engineering, Bioact. Mater. 10 (2022) 15–31.